RESEARCH AND DEVELOPMENT TECHNICAL REPORT
SLCET-TR-90-6

AN OVERVIEW OF MODERN PERMANENT MAGNET DESIGN

HERBERT A. LEUPOLD
ERNEST POTENZIANI II
ELECTRONICS TECHNOLOGY AND DEVICES LABORATORY

AUGUST 1990

US ARMY
LABORATORY COMMAND
FORT MONMOUTH, NEW JERSEY 07703-5000

NOTICE

Disclaimer

The citation of trade names and names of manufacturers in this report is not to be construed as official Government indorsement or approval of commercial products or services referenced herein.

REPORT DOCUMENTATION PAGE

Form Approved
OMB No. 0704-0188

1. AGENCY USE ONLY (Leave blank)	2. REPORT DATE	3. REPORT TYPE AND DATES COVERED
	August 1990	Technical Report: 1970 to 1990

4. TITLE AND SUBTITLE
AN OVERVIEW OF MODERN PERMANANT MAGNET DESIGN

5. FUNDING NUMBERS
PE) 61102A
PR) 1L161102AH47
TA) 01

6. AUTHOR(S)
Herbert A. Leupold, Ernest Potenziani II

7. PERFORMING ORGANIZATION NAME(S) AND ADDRESS(ES)
US Army Laboratory Command (LABCOM)
Electronics Technology and Devices Laboratory (ETDL)
ATTN: SLCET-E
Fort Monmouth, NJ 07703-5000

8. PERFORMING ORGANIZATION REPORT NUMBER
SLCET-TR-90-6

9. SPONSORING/MONITORING AGENCY NAME(S) AND ADDRESS(ES)

10. SPONSORING/MONITORING AGENCY REPORT NUMBER

11. SUPPLEMENTARY NOTES

12a. DISTRIBUTION/AVAILABILITY STATEMENT
Approved for public release; distribution is unlimited.

12b. DISTRIBUTION CODE

13. ABSTRACT (Maximum 200 words)

The high-energy product magnet materials have made possible many (compact, light weight) high-field magnetic flux sources that were not practicable before their advent. Near-revolutionary device consequences are unfolding as a result. This report discusses the approaches to the design of such devices and gives various examples that apply to electron-beam devices, nuclear magnetic resonance, electric motors, and others.

14. SUBJECT TERMS
Rigid permanent magnets; flux confinement cladding; magnetic Ohm's Law; high-energy products

15. NUMBER OF PAGES
71

16. PRICE CODE

17. SECURITY CLASSIFICATION OF REPORT	18. SECURITY CLASSIFICATION OF THIS PAGE	19. SECURITY CLASSIFICATION OF ABSTRACT	20. LIMITATION OF ABSTRACT
Unclassified	Unclassified	Unclassified	UL

Table of Contents

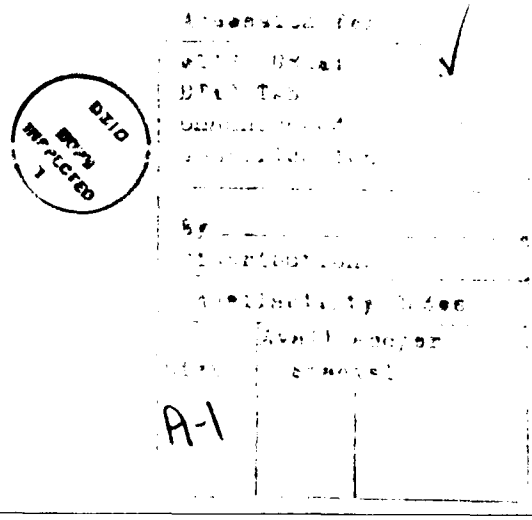

List of Figures

List of Tables

Introduction

The advent of rare-earth permanent magnets (REPM) affords the possibility of fabrication of many novel magnetic structures that are not otherwise practicable.[1,2] So different are these remarkable materials from previous magnets that the conventional design wisdom is inadequate to fully exploit their unique characteristics. Indeed, the conventional wisdom can lead to error or to the employment of cumbersome procedures appropriate for conventional magnets, but unnecessary for REPM's. All of these salutary characteristics stem from two basic attributes of the rare earth-cobalt materials: 1) large intrinsic moments per unit volume (high saturation magnetizations); 2) extraordinarily high resistances to demagnetization by applied fields or demagnetization fields (high coercivities).

The first provides a magnetic field source of high flux density; the second enables the magnet to maintain this flux density in the face of very high demagnetizing fields engendered by low-aspect ratios. Thus, REPM's can, with impunity, be fashioned into shapes that would cause demagnetization of conventional materials. This point is illustrated in Fig. 1, which shows the second quadrant of the hysteresis loop of a typical $SmCo_5$ magnet. Note that the constancy of magnetization to the very high field of $\mu_0 H$ = 1.3 Tesla results in a linear B versus $\mu_0 H$ curve of slope one throughout the entire quadrant. This linearity of the magnetization curve makes possible magnetic structures in which the magnet is exposed to demagnetizing fields well in excess of the remanence. The importance of this property to design simplification will become obvious from the following discussions in which $\mu_0 H$ and $\mu_0 M$ will be written B_0 and M_0 respectively for convenience in curve plotting and calculations. This procedure has the advantage that in the relationship between field, flux density and magnetization , $B = B_0 + M_0$, all three of the principal quantities involved are of the same kind and measured in Tesla. The only drawback of this procedure is that energies are measured in units of $1/\mu_0$ of a joule. This is a small inconvenience since explicit energies are rarely involved in magnetic design.

Magnetic circuit design with the older magnetic materials, such as alnico, is largely an intuitive hit-or-miss affair, as is clear from the B vs B_0 curve for alnico in Fig. 1. Flux densities are low for all but geometries with the very highest B to B_0 ratios; that is, those with the very lowest demagnetization coefficients. Because the state of magnetization of each magnet is dependent upon the geometry of the structure in which it is placed, exact analytic solution for all but the simplest configurations is very difficult or impossible. Hence, a great deal of reliance is placed on numerous approximations, actual physical models, electric analogues, or rules of thumb.

Because of the analytical simplification afforded by the rigidity of the REPM's, the range of applicability of the traditional approaches to magnetic design has been greatly extended. These approaches fall into four broad types: 1) analogy of magnetic configurations to electrical circuits; 2) analytical solutions through Maxwell's equations;

3) reduction of permanent magnet arrays to distributions of equivalent charge densities and current sheets and the insertion of those distributions into Coulomb's law; and 4) brute-force computer solution of tentative configurations, the plausibilities of which are previously established by one of the other approaches, usually the first. We will now discuss these approaches and employ them to solve illustrative problems.

The Magnetic Analogue of Electric Circuit Theory

In the not-too-distant past, elementary courses in general physics almost invariably included a brief treatment of magnetic circuits that featured a rather simplistic derivation of a magnetic analogue of Ohm's law. In this scheme, the role of electric current I is played by the magnetic flux Φ, that of the electromotive force V by magnetomotive force F, the electric conductance G by the magnetic permeance P, and the resistance R by the reluctance R, so that the magnetic Ohm's law reads:

$$\Phi = PF \tag{1a}$$

or

$$\Phi = F/R, \tag{1b}$$

in respective correspondence to

$$I = GV \tag{1c}$$

and

$$I = V/R \tag{1d}$$

in the familiar electrical Ohm's law. Permanent magnets can then be regarded formally as magnetic "batteries," and materials of high permeability, such as soft iron or permalloy, as essentially perfect flux conductors, in analogy to the "perfect" current conductor, copper, in electrical circuits. Air gaps and materials of low permeability play the role of magnetic resistors. The analogy is completed by the identification of electrical solenoids wound about permeable circuit members with flux "generators," which can be either ac or dc, depending upon the currents sent through them.

Although this approach, like most analogies, is philosophically and mnemonically gratifying, it was rarely used in practice as outlined, and now is often deleted from the elementary courses. The barrier to more general usefulness was essentially twofold. In the first place, unlike electric currents, magnetic fluxes are not confined to neat, analytically tractable paths like wires, but fill virtually all of space. This difficulty is not too serious, because the space around a magnetic circuit can, in many cases, be divided into flux paths of which the boundaries are planes, cylindrical arcs, or segments of

spherical surfaces that emanate normally from the surfaces of the circuit to connect points of different magnetic potential. The permeances of these simplified paths can be calculated approximately through standard formulae, and if the division has been made judiciously, surprisingly good approximations to the true fluxes can often be obtained. Figure 2 shows some frequently used flux paths together with the formulae used to calculate their permeances.

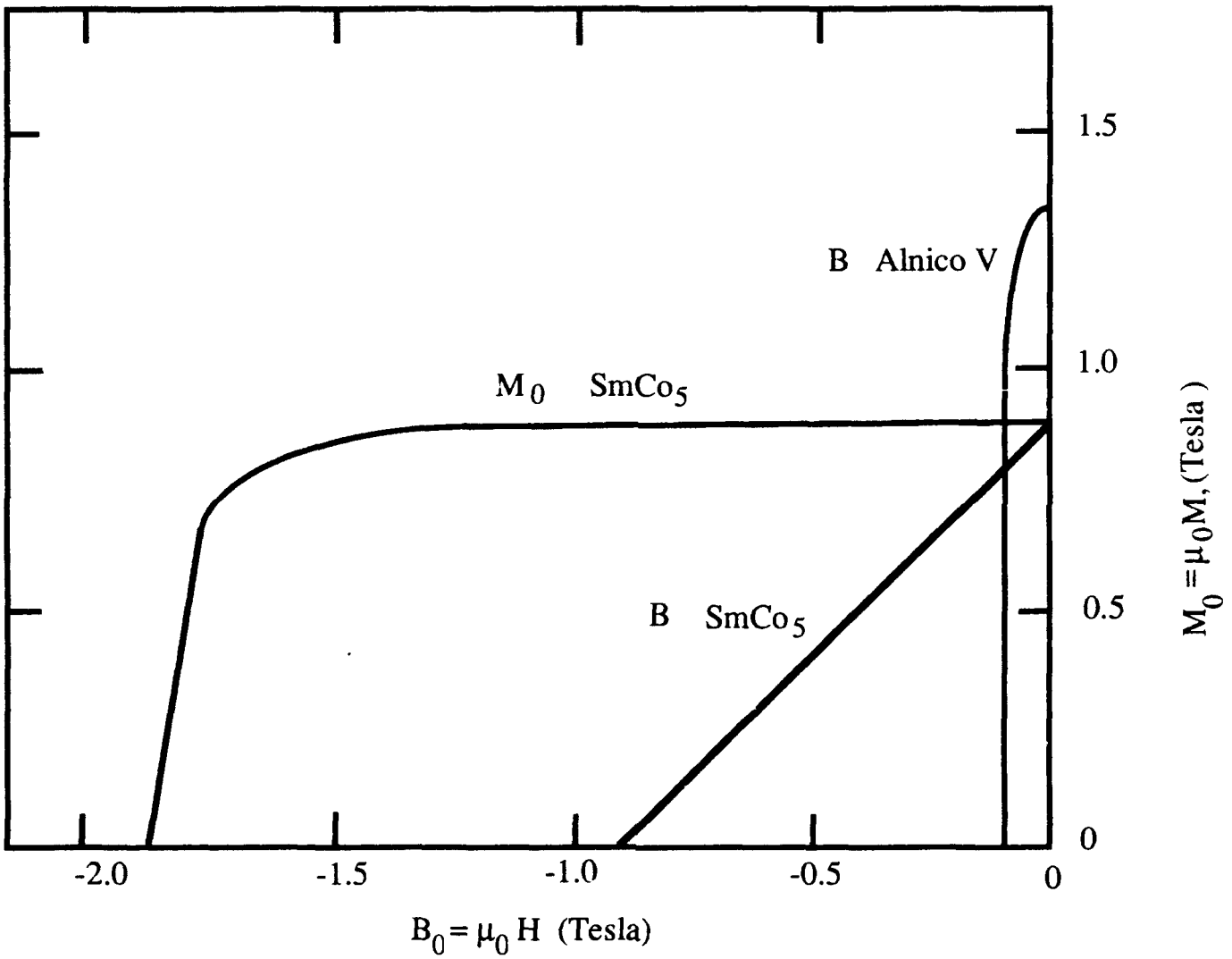

Figure 1. Demagnetization curves for $SmCo_5$ and alnico V magnets.

The second, and more serious, difficulty that has prevented a simple, direct application of the magnetic Ohm's law is that conventional permanent magnet materials, such as the alnicos, generate no unique magnetomotive force (mmf), because their mmf's depend upon the circuits into which they are inserted. The great value of REPM's in the simplification of circuit design arises because these materials exhibit the same total circuital mmf, regardless of the natures

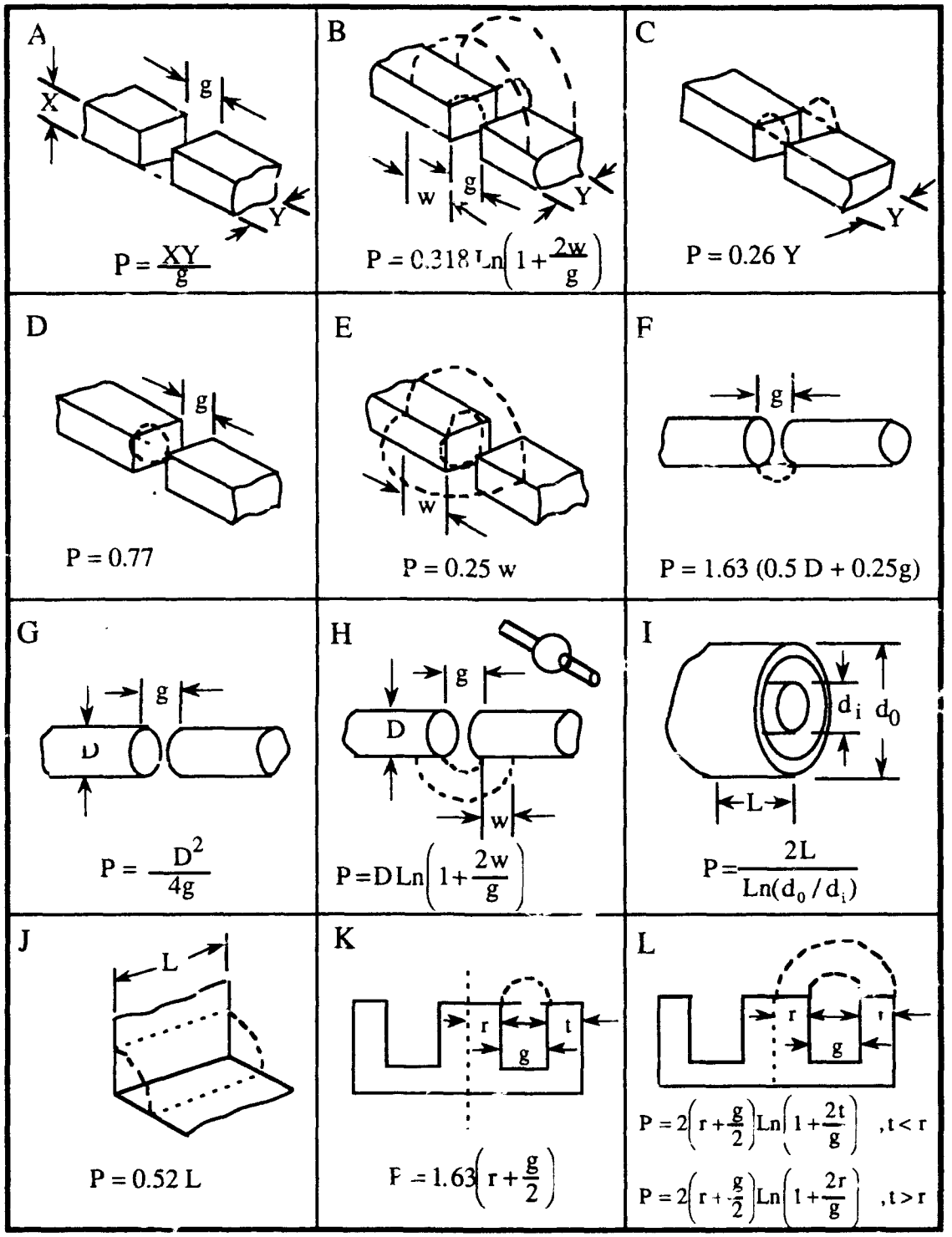

Figure 2. Standard permeances

of the circuits in which they find themselves. Although this advantage has been discussed previously,[1-3] it is still not as widely appreciated as are the high energy products and coercivities of the REPM's; consequently, circuits employing these materials are still often analyzed by the same cumbersome procedures that are necessary when conventional materials are employed.

To illuminate the origins of these difficulties and to highlight the contrasts between the cobalt rare earths and conventional magnets, it is useful to consider the derivation of the magnetic Ohm's law. We begin by writing the circuital form of Ampere's law

$$\oint \vec{H} \cdot d\vec{s} = \pm I \tag{2}$$

where the magnetic field H is in amps/meter, the current I, linked by the loop integral, is in amperes, and the sign depends upon whether the current direction in the coils produces an mmf aiding or opposing that of the magnet. Assuming H_m is the average field over the length of the path in the magnet L_m, we can write

$$H_m L_m + \int_A^B \vec{H}_L \cdot d\vec{s} = \pm I \tag{3}$$

where A and B are the ends of the magnet, the line integral is along a flux line outside of the magnet, and H_L is the field along that line. Outside the magnet, $\mu_L H_L = B_L$, therefore

$$H_m L_m + \int_A^B \frac{\vec{B}_L \cdot d\vec{s}}{\mu_L} = \pm I \tag{4}$$

but

$$B_L = \frac{d\Phi(r)}{dA} \tag{5}$$

where dA is a differential element of area normal to a flux line of differential length ds and $d\Phi(r)$ is the flux passing through it. Consequently,

$$H_m L_m + \int_A^B \frac{d\Phi}{dA} \frac{ds}{\mu_L} = \pm I \tag{6}$$

$$H_m L_m + \int_A^B \frac{d\Phi}{\mu_L dA} ds = \pm I \tag{7}$$

Of course, the area dA and permeability μ_L associated with flux $d\Phi$ may vary with progression along the flux line, but if we denote their average product by $\overline{\mu_L dA}$ and write

$$\overline{\left(\frac{d\Phi}{\mu_L dA}\right)} = \frac{d\Phi}{\overline{\mu_L dA}}$$

and

$$\frac{ds}{\overline{\mu_L dA}} = \frac{1}{dP_t^E} \tag{8}$$

where P_t^E is the total permeance of the circuit exclusive of the internal permeance of the magnet, then, Eq. (7) becomes

$$H_m L_m + \frac{d\Phi}{dP_t^E} = \pm I \tag{9}$$

$$\frac{d\Phi}{dP_t^E} = \pm I - H_m L_m \tag{10}$$

Integration of all fluxes yields

$$\Phi_t / P_t^E = \pm I - H_m L_m \tag{11}$$

where Φ_t is the total flux Φ_m emanating from the magnet; therefore,

$$\Phi_m = \Phi_t = P_t^E [\pm I - H_m L_m] . \tag{12}$$

However,

$$\Phi_m = B_m A_m \tag{13}$$

where B_m is the average flux density within the magnet, and by substitution of (13) in (12) we obtain

$$B_m = P_t^E [\pm I - H_m L_m] / A_m \tag{14}$$

For $SmCo_5$ the demagnetization curve is reversible, linear, and of the form

$$B_m = \mu_R H_m + B_R \quad , \tag{15}$$

where μ_R is the recoil permeability and B_R is the remanence flux density, $\mu_0 M_R$. Solving (13) and (15) for H_M, we obtain

$$H_m = (B_m - B_R) / \mu_R = \Phi_m / \mu_R A_m - B_R / \mu_R \quad . \tag{16}$$

Multiplication of (14) by A_m and combination of the results with (16) yields

$$\Phi_m = P_t^E [-\Phi_m L_m / \mu_R A_m + B_R L_m / \mu_R \pm I] \tag{17}$$

$$\Phi_m = \frac{(B_R L_m / \mu_R \pm I)}{(1 / P_t^E + L_m / \mu_R A_m)} \tag{18}$$

or

$$\Phi_m = \frac{(B_R L_m / \mu_R \pm I)}{(R_t^E + R_m)} \quad . \tag{19}$$

This is the magnetic form of Ohm's law where the total flux Φ_m is analogous to the total current and the reluctances R_t^E and R_m correspond to the total circuit resistance external to the battery and the battery internal resistance, respectively. Corresponding to the battery emf is $L_m B_R / \mu_R$ or $-L_m H_C$ and $\pm I$ is the analogue of the emf from a zero impedance, constant voltage source. This simple and useful formula is applicable to cobalt-rare earth magnets because of the linear relationship between H_m and B_m expressed by Eq. (15) which, in turn, is a consequence of the constancy of magnetization in all parts of the magnet, regardless of stimuli arising from the rest of the circuit or the magnet's own geometrical peculiarities. In contrast, conventional magnetic materials do not have reversible demagnetization curves that are expressible in simple analytical form. Therefore, in dealing with circuits containing such magnets one must proceed less directly and with recourse to B-H graphs such as those shown in Fig. 3. For simplicity, we consider as an example a circuit with no electromagnetic sources of flux. In such a case, Eq. (14) can be written:

$$B_m / H_m = L_m P_t^E / A_m \tag{20}$$

Then, one must calculate P_t^E which, together with the use of magnet length and the cross-sectional area in (20), yields B_m/H_m. Next, a "load line" with slope B_m/H_m is drawn through the origin and its intersection with the second quadrant B-H curve determines B_m. The product $B_m A_m$ then yields Φ_t, which is the total flux output of the magnet; Φ_t is distributed among the various flux paths in the circuit in accordance with Ohm's and Kirchoff's laws.

If the demagnetization field of the conventional magnet is lessened by an increase in P_t^E resulting from the narrowing of an air gap within the circuit, the operating point of the magnet moves along an approximately linear minor loop to point B in Fig. 3, in

accordance with the new value of B_m/H_m. When changes in the circuit are such as to move the operating point from left to right on the minor loop, we can use an expression such as (15) with the intercept of the minor loop with the B axis, B_i in place of B_R, and the slope of the minor loop μ_i in place of μ_R. Consequently, one may define a magnet mmf of the same form as that for the cobalt rare earths, i.e.,

$$F = B_i L_m / \mu_i \quad . \tag{21}$$

However, should the demagnetization field increase due to a widening of an airgap, temporary removal of the magnet from the circuit, or application of an external demagnetizing field, the operating point would move to the left along the demagnetization curve to C, the base of a new minor loop CD. The magnet would also have a new mmf given by the new line constants B_i' and μ_i'

$$F = B_i' L_m / \mu_i' \quad . \tag{22}$$

Hence, we see that no unique mmf can be assigned to a conventional permanent magnet, and if the useful magnetic field is to be modulated by variation of gap length or electrically generated mmf's, the magnet mmf will always be that corresponding to the lowest point on the demagnetization curve reached in the course of the modulation cycles. An additional complication in determining the mmf of a conventional magnet is that the lengths L_m appearing in Eqs. (21) and (22) are effective rather than actual lengths. Because of demagnetization fields, the magnetization of conventional magnets tends to be nonuniform, which means that different parts of the magnet lie on different load lines, and therefore produce different mmf's and inhomogeneous fields. This causes effective lengths to be shorter than actual ones and all the other germane quantities, such as H_M and B_M, to have only a rough average significance. For some configurations, use of geometrical lengths and average field values can cause significant errors, and estimations of effective lengths must be made. For an example, see Ref. 4. Magnetic quantities and their electric analogues are summarized in Table 1.

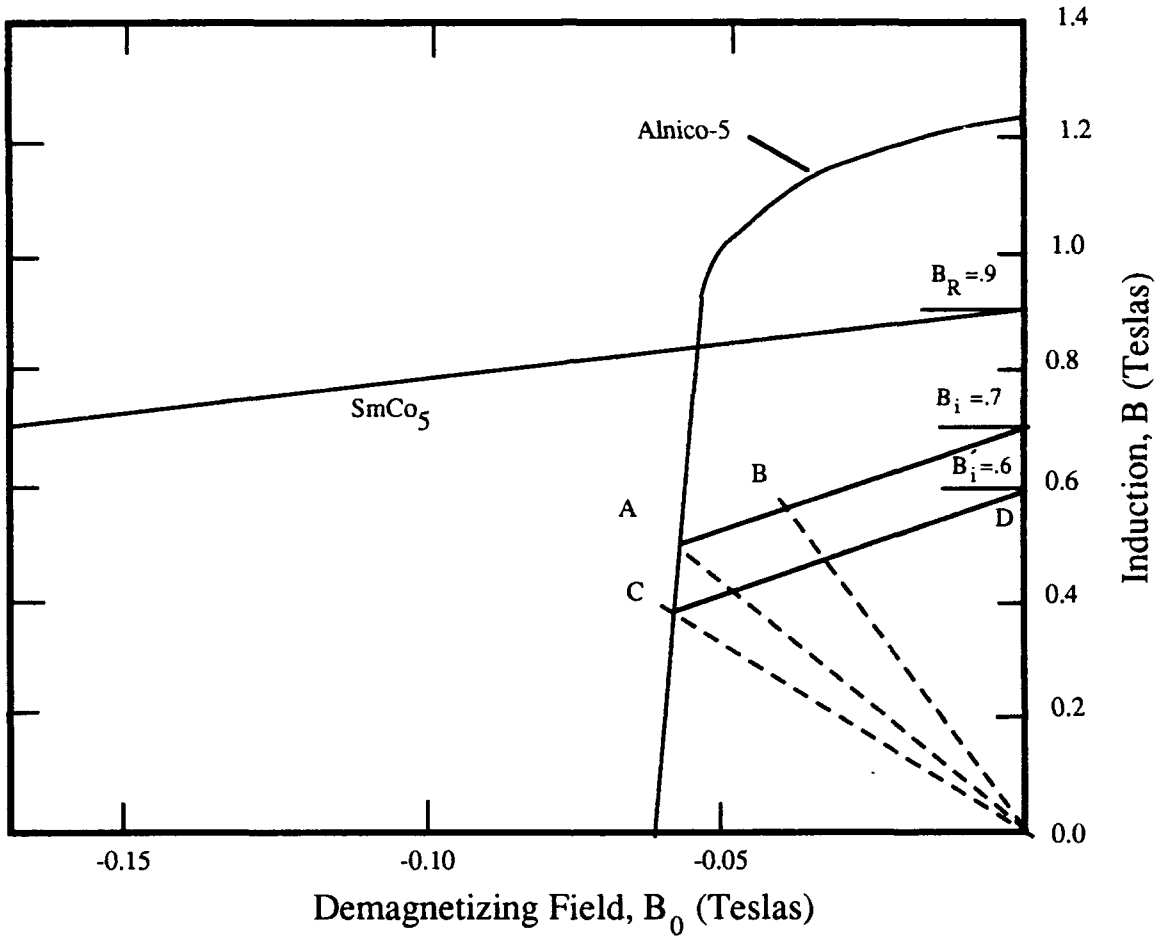

Figure 3. Determination of B_m in an Alnico V magnet. The load line OA is determined from the total external permeance as described in the text. B_m is the value of B at intersection A. A decrease in P_t^E would lower the operating point to C, the base of a new reversible minor loop CD. The reversible linear demagnetization curve for $SmCo_5$ magnets of 0.9 Tesla is shown for purposes of comparison.

Table 1. Magnetic Circuits and Their Electrical Counterparts

MAGNETIC			ELECTRIC		
Magnetomotive Force	$\Delta U, F$	Amperes	Electromotive Force	$\Delta V, \mathcal{E}$	Volts
Magnetic Potential	U	Amperes	Electric Potential	V	Volts
Magnetic Flux	Φ	Webers	Electric Current	I	Amperes
Permeance	P	Webers/Ampere	Conductance	G	Siemens
Reluctance	R	Amperes/Weber	Resistance	R	Ohms
Magnetic Field	H	Amperes/m	Electric Field	E	Volts/m
Flux Density	B	Teslas	Current Density	J	Coulomb/m^2-sec
Permeability	μ	Tesla-m/Ampere	Conductivity	σ	Siemens/m
Magnetic Field Energy	W	Joules	Electric Power	P	Watts
MMF of a Magnet	$L_M H_C$	Amperes	EMF of a Battery	V_B	Volts

Illustrative Example of Contrasting Magnetic Gap Field Calculations for a Circuit Employing $SmCo_5$ and the Same Circuit Using Alnico V

In Fig. 4(a) is pictured a simple magnetic circuit with the space around it divided into permeance paths as described in the introduction. The flux and field of interest is that in the magnet gap P_G. To calculate these quantities we must first find the permeances associated with the fourteen external flux paths. All are of standard form and can be calculated by means of formulae found in Fig. 2 and in Refs. 3-6. To aid in the visualization of the forms of these paths, brief descriptions of each are summarized in Table 2. The fourteen permeances are in parallel with each other and in series with the internal permeance P_m of the magnet. (See Fig. 4(b).) Almost rigid magnets ($B_R / B_{0C} = 1.05$) of $B_R = 0.9$ Tesla are employed. From the values of the quantities shown, the total circuit reluctance is calculated to be $R_t = R_m + R_t^E = 0.3115 + 0.035 = 0.346\ m^{-1}$. The mmf: $F = L_m B_0 = L_m B_R / 1.05 = 3.96\ B_R / 1.05 = 3.77\ B_R = 3.39$ Tesla-m. Here, as previously stated, we use B_0 rather than H so that $F = L_m B_0$ .is really a quasi-potential measured in Tesla-meters. There is no difficulty involved when this value is used to obtain a flux via the formula $\phi_t = P_t F$ because the true $F(true) = B_{0C} L_m / \mu_0$ and the true P is

$$P(true) = \mu_0 \sum_P \mu_P \frac{A_P}{L_P}$$

where μ_P is the permeability relative to empty space and where the $\mu_P A_P / L_P$'s are the relative permeances of the individual external flux paths

$$\phi_t = P_t(true)\, F(true) = \left(\sum \mu_P \mu_0 \frac{A_P}{L_P} \right) \left(\frac{B_{0C} L_m}{\mu_0} \right)$$

$$\phi_t = B_{0C} L_m \sum_P \mu_P \frac{A_P}{L_p}$$

so that when $B_{0C} L_m$ is used for the potential F, and the relative permeability, $\sum_P \mu_P A_P / L_P$, for P_t the same results are obtained as from the true values of F and P_t. In most problems μ_P is either equal to 1.0, as in air gaps and in "rigid" permanent magnets, or to ∞, as in iron yokes and pole pieces.

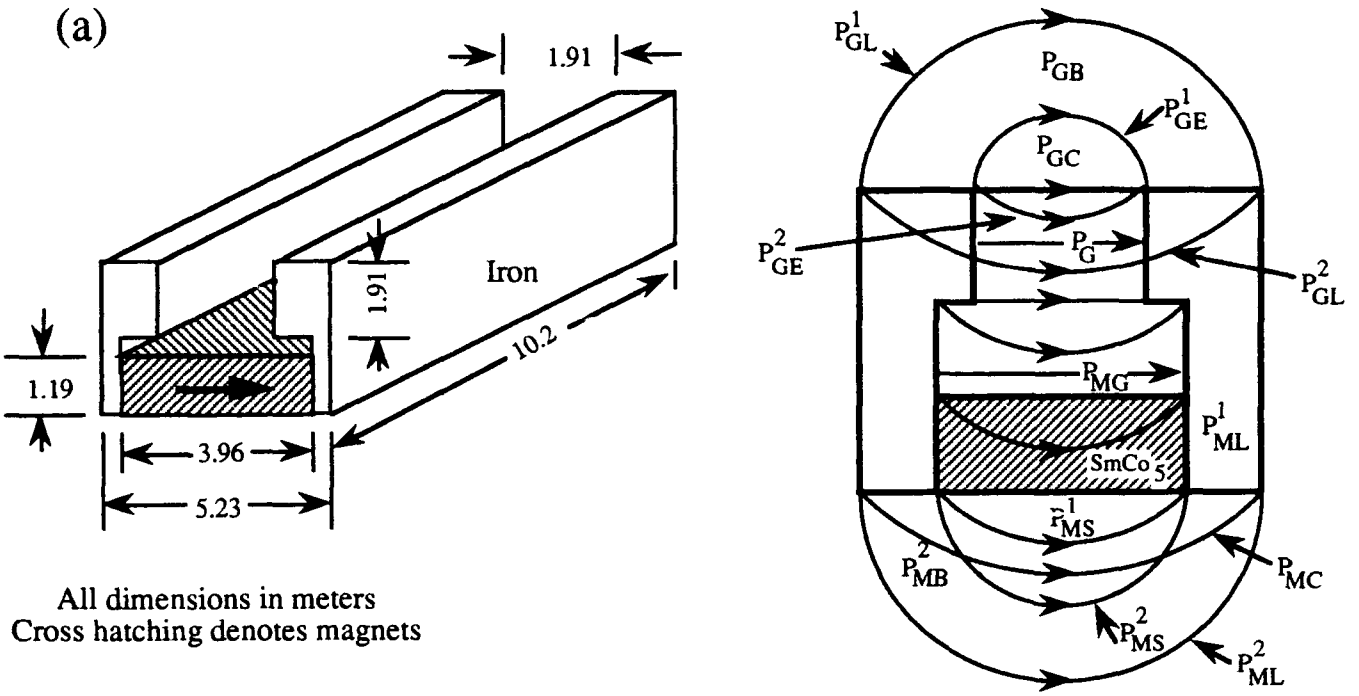

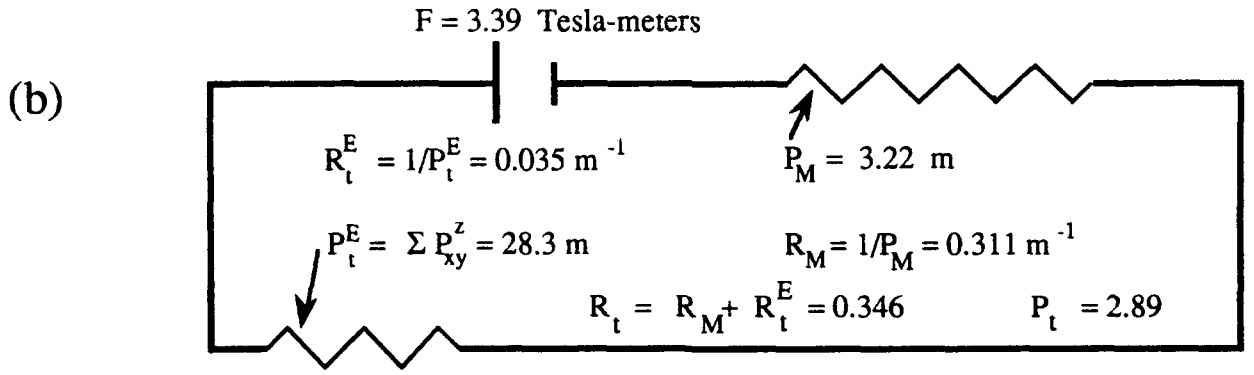

Figure 4. (a) Division of space around magnetic circuit into approximate flux paths. (b) Schematic of equivalent electric circuit.

Therefore we find the total flux emanating from the magnet:

$$\Phi_t = F/P_t = 3.39 / 2.89 = 9.8 \quad .$$

Since all permeances in P^E_t are in parallel, the gap flux is given by:

$$\Phi_G = P_G \Phi_t / P^E_t = (10.2)(9.8) / 28.3$$

Table 2. Magnetic Flux Paths of Figure 4(a)

PATH DESCRIPTION	PATHS	FORMULAE
Gaps With Opposing Parallel Faces	P_{MG}, P_G, P_M	$P = A_G / t_G$
Paths Between Parallel Linear Edges of Opposing Surfaces	P^1_{GE}, P^2_{GE}	$P = 0.26\ L$
Annular Cylindrical Sections Extending Between Coplanar Surfaces	P^1_{ML}, P^2_{ML}, P^1_{GL}, P^2_{GL}	$P = 0.318\ \ln(1+2t/L_G)$
Spherical Quadrants ("Orange Slices") Connecting Opposing Corners of Opposing Parallel Surfaces	P_{GC}	$P = 0.77\ L_G$
Semicylindrical Sections Backstreaming from the Sides of the Magnet	P^1_{MS}, P^2_{MS}	$P = 0.318\ y$
Quadrants of Spherical Shells ("Melon Slices")	P_{GB}, P_{MB}	$P = 0.25\ t$
"Orange-Slice" Sections Backstreaming from Longitudinal Edges of Magnet	P_{MC}	$P = L / 8$

IN THE FORMULAE: A_G and L_G refer to gap cross-sectional areas and lengths, respectively; t to thicknesses of cylindrical and spherical shells, L to lengths of edges from which flux paths emanate, and y to the perimeter of the magnet.

Calculated Values of Permeances in Meters

$P_{MG} = 1.82$	$P^1_{GL} = 3.18$	$P_{GC} = 0.292$	$P^2_{MS} = 0.759$
$P_G = 10.16$	$P^2_{GL} = 1.19$	$P_{GB} = 0.795$	$P_{MC} = 0.495$
$P^1_{GE} = 2.64$	$P^1_{ML} = 1.52$	$P_{MB} = 0.320$	$P_M = 3.22$
$P^2_{GE} = 0.991$	$P^2_{ML} = 0.904$	$P^1_{MS} = 3.23$	$P^E_t = 28.3$

$P_t = 2.89$

and the average field in the gap

$$B_G = \Phi_G/A_G = 3.53/19.4 = 0.182 \text{ Teslas.}$$

If the calculation were to be made for the same configuration with the $SmCo_5$ replaced by alnico V, one would proceed as follows:

(1) Calculate the total external permeance $P_t^E = 28.3$ m and total circuit permeance $P_t = 2.87$ m.

(2) Find the ratio B_m/B_{0m} via the formula

$$B_m/B_{0m} = -L_m P_t^E / A_m = -(3.96)(28.3)/12.1 = -9.26 \quad .$$

(3) Draw the line $B_m/B_{0m} = -9.26$ together with the second quadrant of the alnico V demagnetization curve (Fig. 3).

(4) Find the magnet operating point at intersection (A) and the value of B_m at that point, i.e., $B_m = 0.514$ *Teslas, as in Fig. 3.*

(5) Calculate total flux $\Phi_t = B_m A_m = 6.23$ Webers.

(6) Find $\Phi_G = P_G \Phi_t / P_t^E = 2.21$ Webers.

(7) Find $B_G = \Phi_B/A_G = 0.114$ Teslas.

We see that the first and last two steps in this calculation must also be completed for $SmCo_5$ and Φ_t obtained from $\Phi_t = F/\mathcal{R}_t$ in lieu of step (5). But the time-consuming steps, (2) to (4), are unnecessary when REPM's are used, and no external aids such as graphs are needed.

Magnetic circuit design by means of the electric circuit analogue, although seemingly crude, yields valuable qualitative guides to design adjustment and, in many cases, good quantitative results as well. The latter are often surprisingly accurate, especially when the calculated quantities of interest involve averages over large areas, as is the case of magnetic flux calculation. If a local field or flux density calculation is made, agreement of calculated values with actual values is not as good. These points are illustrated in Fig. 5. Note the remarkable agreement in geometric detail between the rough permeance calculations and the computer plot of Fig. 14. Point A is the point

which, according to the calculations, is the demarcation between the flux lines which go from limb to wall and those which return to the other end of the limb. Point B is the calculated effective equator of the magnet. Note how it is the approximate symmetry center for the P_o flux lines. Point C is the calculated point that marks the switching of the center post flux lines from the permeable plate to the ring magnet. Point D is the predicted switch-over point from P_r paths to P_B paths. The Φ obtained from these calculations was 2.12×10^{-5} webers, compared with the 2.18×10^{-5} Webers yielded by our longhand permeance calculations, agreement to within less than two percent. In contrast, calculations of the flux density at Point E yield 0.39 Teslas for the analogue method and 0.30 Teslas for the computer, an approximately 30 percent disagreement.

Significance of the Energy Product

The magnetic circuit analogue to electric power is magnetic field energy. Both quantities are maximized when the source impedance is equal to the external load impedance. For the magnetic case, this occurs when R_E is equal to R_m and P_E is equal to P_m. Here R_E and R_m are the reluctances of the external load and the interior of the magnet, respectively, and P_E and P_m are the respective permeances. P_E is the sum of the gap and leakage permeances P_G and P_L.

For an electrical circuit the external power is $P_E = V_E I_E$.

For a magnetic circuit the analogue is the stored external energy

$$E_E = F_E \Phi_E. \tag{23}$$

But $\Phi_E = \Phi_m$

and for impedance match

$$F_E = F_m,$$

so that $$E_E = F_m \Phi_m = H_m L_m B_m A_m = H_m B_m V_m, \tag{24}$$

where V_m is the volume of the magnet.

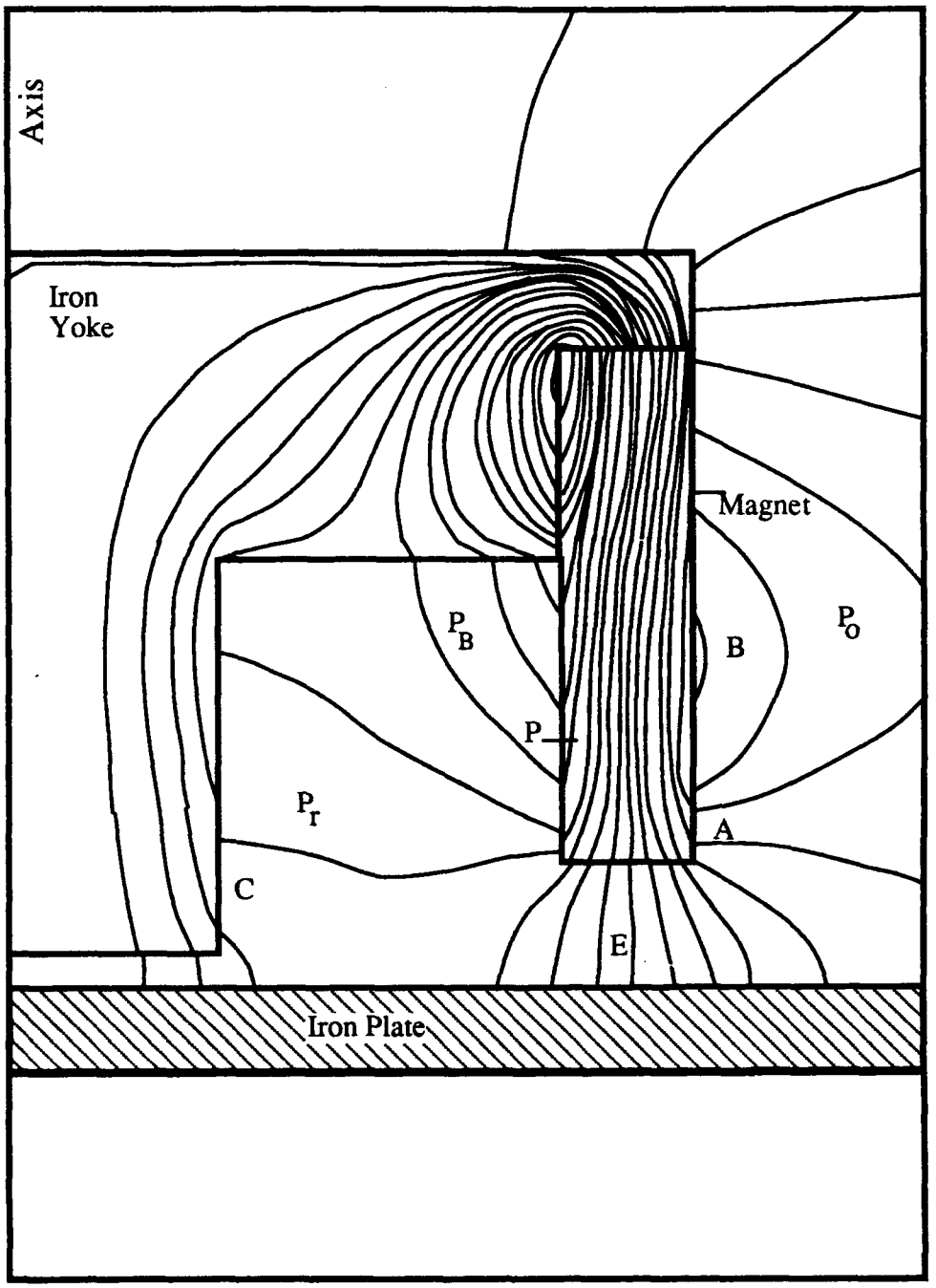

Figure 5. Computer plot of flux lines produced by a cylindrically symmetric speaker magnet of E-shaped cross section in proximity with an iron plate.

For a magnet with a reversible demagnetization curve such as the REPM

$$B_m = \mu_R H_m + B_R$$

$$E_E = H_m B_m V_m = [\mu_R H_m^2 + B_R H_m] V_m \qquad (25)$$

and the energy is maximum when

$$0 = \frac{dE_E}{dH_m} = 2\mu_R H_m + B_R$$

and $$H_m = - B_R / 2\mu_R = H_c / 2 \qquad (26)$$

and

$$B_m = B_R / 2 \qquad (27)$$

Insertion of (27) into (25) yields

$$E_E^{MAX} = \frac{B_R H_c V_m}{4} \qquad (28)$$

so that the energy is proportional to the quantity

$$B_R H_c / 4 \quad , \qquad (29)$$

called the energy product, which is measured in megagauss-oersteds in Gaussian units and in Joules in SI. It is a measure of the maximum energy a material is capable of storing in an external field and is, therefore, a convenient figure of merit for permanent magnets. It is not, as is sometimes believed, a measure of the maximum attainable external field. It is a measure not only of how large a field is attainable, but also of the useful spatial volume over which it is obtained. Both field and volume are taken into account in the maximum stored energy density and in the energy product to which it is identical.

Flux Confinement by Cladding

Experience in magnetic design teaches us that, in most magnetic circuits, much of the flux generated by the permanent magnets is wasted by distribution among unwanted flux paths exterior to the work space of interest. The electric analogue method suggests a

solution to this problem. In an electrical circuit, current can be kept from flowing along extraneous paths either by insulation of those paths from the desired routes or by employment of compensating or "bucking" potentials, as in a potentiometer. Pending the advent of room temperature superconductors with sufficiently high lower critical fields (H_{c1}), magnetic insulation is not practicable at present. However, with rigid magnets such as the REPM, the potentiometric method has proved to be very fruitful in magnetic design.

In illustration, let us consider the simplest of magnetic circuits — that of a horseshoe configuration, as in Fig. 6. Clearly, much of the generated flux leaks through regions P_L. The equivalent current in the electric analogue flows through wires G_L. The analogy is not exact, since the G_L are discreet, while the P_L are continuous. However, this slight discrepancy is not relevant to illustration of the principle of cladding. In the electric circuit, batteries V_c of the appropriate EMF are placed in G_L, so that no current flows there. To effect the analogous suppression of flux flow in P_L of the corresponding magnetic circuit, it is clear that permanent magnets F_c analogous to the batteries V_c must be placed in P_L to suppress the flux flow there. To find the appropriate design parameters, we begin by assuming that this goal has already been accomplished and then work backwards from the desired conditions. By the hypothesis of confinement, the total flux furnished by the magnets flows exclusively within the cross section of the pictured circuit and is given by the magnetic Ohm's law:

$$\Phi = F / R_t = -2L_m B_{0C} / (R_m + R_G)$$

$$\Phi = 2 L_m B_R / (R_m + R_G), \qquad (30)$$

where L_m is the length of a single magnet, B_R is the magnet remanence, R_m and R_G are the reluctances of the magnets and gap, respectively, and B_{0C} is the coercivity, which for our perfectly rigid magnets is equal to $-B_r$. The reluctivity of the magnets is assumed to be one, and that of the yoke, zero. For total flux confinement to be effected, every point on the surface of, or exterior to the final configuration, must be at the same potential. This condition is fulfilled automatically for points on the equipotential surface of the iron yoke. Therefore, cladding must be placed around the magnets and the gap so that its outer surface potential is everywhere equal to that at the yoke surface. Therefore, the potential difference between any point C on the cladding surface and point A on the yoke must be equal to zero and given by the line integral along any path connecting A and C. We consider the path A B C shown in Fig. 7.

$$F_{ABC} = F_{AB} + F_{BC} = 0 \qquad (31)$$

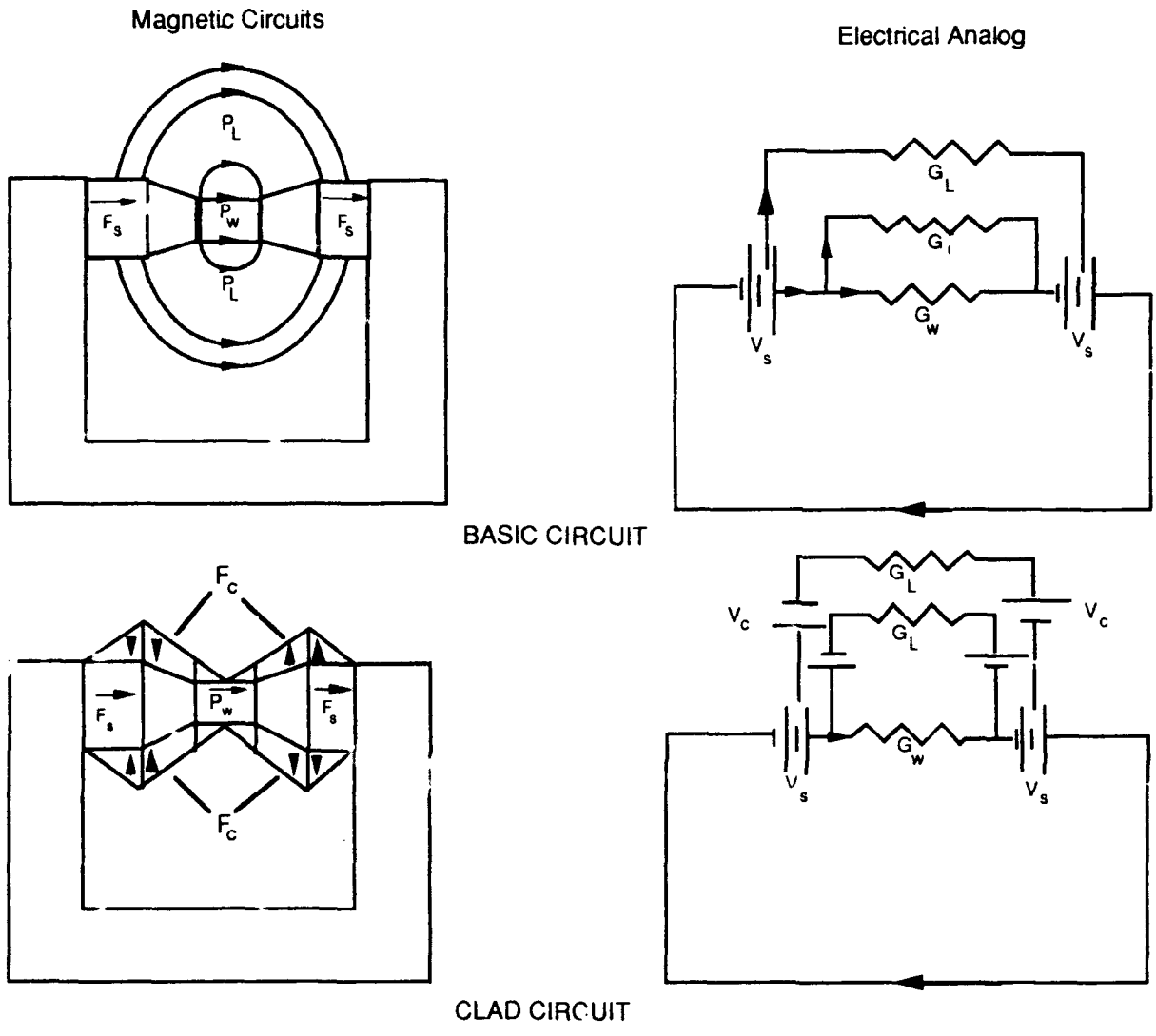

Figure 6. Gap field intensification through cladding.

$$F_{AB} = F_m X_B / 2L_m \,. \tag{32}$$

where F_m is twice the mmf across one of the magnets and F_{BC} is given by:

$$F_{BC} = B_{0d} Y_{BC} \quad , \tag{33}$$

where B_{0d} is the radial magnetic field in the cladding and Y_{BC} is the cladding thickness at point B. Combining expressions 31, 32 and 33 with

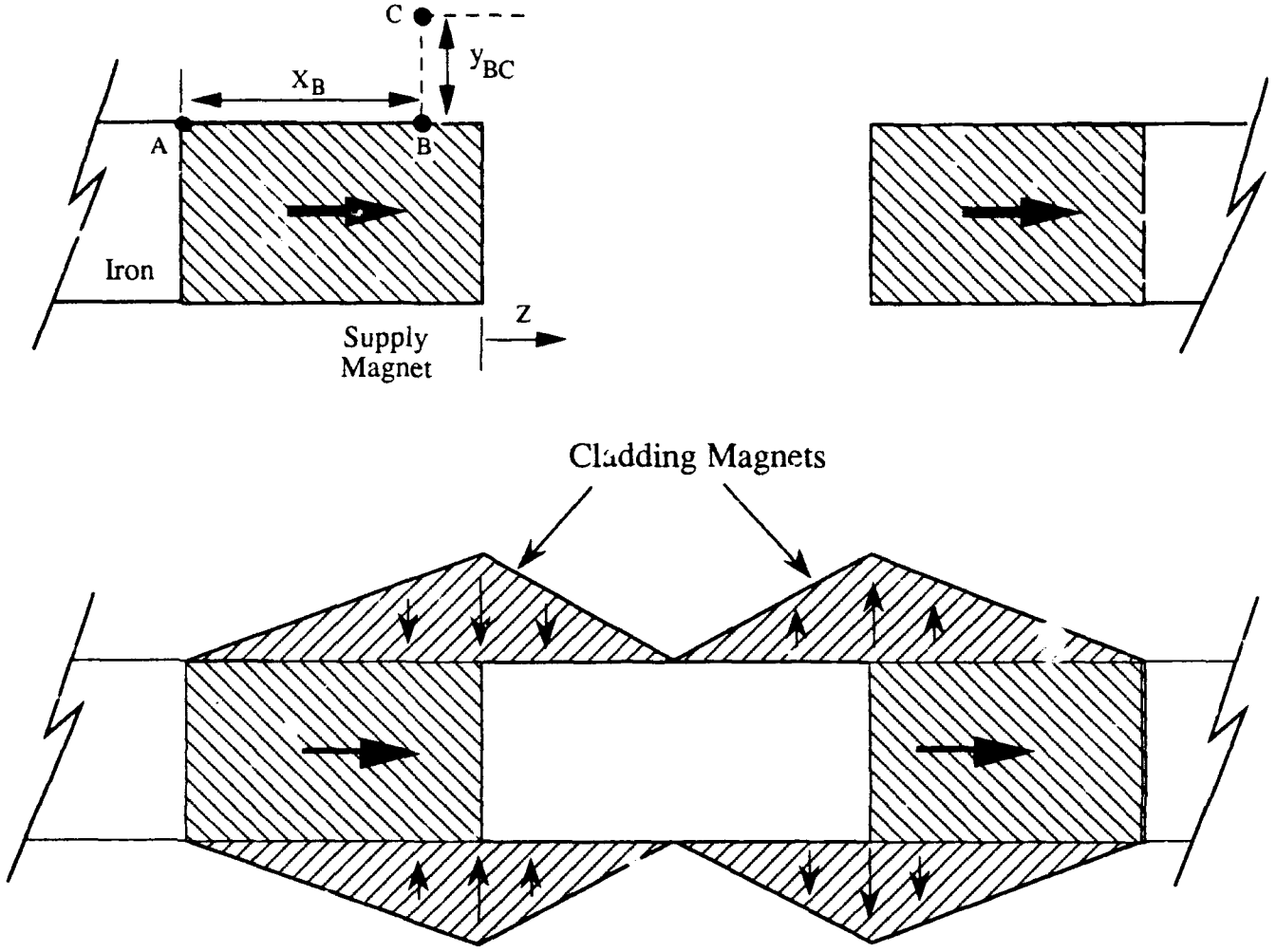

Figure 7. Determination of cladding thickness of a horseshoe magnet in the gap region.

$$F_m = \Phi R_m \tag{34}$$

$$0 = \Phi R_m X_B / 2L_m + B_{0d} Y_{BC} \tag{35}$$

Substitution of 30 in 35 yields

$$Y_{BC} = F_{BC} / B_{0d} = -F_{AB} / B_{0d} = -\Phi R_m X_B / 2L_m B_{0d} \tag{36}$$

Since, by hypothesis, no flux flows to the exterior, the radial flux density in the cladding magnet must also be zero. From the demagnetization curve of a magnetically rigid material, we know that at zero flux density, the field is equal to the coercivity $B_{0c} = -B_r$. Substitution of this value for B_{0d} in Eq. (36) yields

$$Y_{BC} = 2L_m B_r R_m X_B / 2L_m B_{0C} (R_m + R_G) = \frac{R_m X_B}{(R_m + R_G)} \qquad (37)$$

and the outer surface of the cladding about the supply magnet is a truncated cone, the half angle of which has a slope of $R_m / (R_m + R_G)$. The cladding thickness Y reaches maximum at the end of the magnet, which is at the gap edge. The thickness declines beyond the edge because the field in the gap B_{0G} is in the direction opposite to that of B_{0m} and it is given by

$$B_{0G} = B_G = B_m = \Phi / A_M \ , \qquad (38)$$

where A_m is the cross-sectional area of the gap. The potential declines with distance from the gap edge z as

$$F = - zB_{0G} = zB_m = z \Phi / A_m \quad . \qquad (39)$$

Inserting (30) for Φ we obtain

$$F = -2zL_m B_r / A_m [R_m + R_G] \qquad (40)$$

At midgap the potential goes through zero and takes on increasingly negative values beyond. The negative potentials are balanced by cladding of opposite polarity, which increases in thickness up to the other gap edge, after which it declines linearly to zero. The resulting antisymmetric structure is shown in Fig. 7. In practice, the gap cladding is sometimes omitted for easier access. This results in a reduction in gap field and some bowing of the field lines. This is often tolerable, but becomes more serious as the gap length increases.

The efficacy of cladding is demonstrated by a consideration of the unclad structure and its identical clad counterpart in Fig. 6. The latter has a gap field of 2 Teslas, as compared with only 0.8 Teslas for the unclad structure. The 2.2 Teslas delivered by the clad version compares favorably with that usually delivered by electromagnets that are many times as large, and is generated without power supply or current source. Cladding is especially effective when the leakage permeances are a large fraction of the total external permeance. When the same horseshoe structure has no tapered pole pieces as in Fig. 7, most of the external permeance is in the gap and cladding raises the gap field from 0.5 Teslas to only 0.8 Teslas.

Clad Permanent Magnet Solenoids

Traditionally, uniform magnetic fields extending over distances that are long, compared to the diameter of a cylindrical working space, are produced by electrical

solenoids. These are cumbersome, require power supplies, and often entail the expenditure of considerable energy. The rare-earth materials afford provision of solenoidal fields with permanent magnet structures. A particularly useful and ingenious design for such a configuration was conceived by Neugebauer and Branch[7] to focus the electron beam in a microwave klystron. (See Fig. 8.) The required flux density was to have a magnitude of 0.15 Teslas and a direction parallel to the axis of a cylindrical space 21.6 cm long and 6.99 cm in diameter. The $SmCo_5$ magnet supplying the flux is in the form of an axially magnetized annular shell with μ_r equal to one forming the perimeter of the work space. Abutting against its ends are disks of a passive ferromagnet of high permeability and saturation magnetization, such as iron or permalloy. These disks serve as pole pieces to lead the flux produced by the magnet into the cylindrical work space. Again, we assume that all of the flux generated by the magnet passes through the work space. To accomplish this, the magnet must have a cross-sectional area A_m dictated by conservation of flux, viz:

$$B_m A_m = B_w A_w = B_{0w} A_w \tag{41}$$

where B_m is the flux density in the magnet and B_w that in the work cavity, and where A_w is the cross-sectional area of the cavity. If, as we assume, flux confinement has been accomplished, and since the end discs are equipotential surfaces, the field in the magnet B_{0m} must equal B_{0w}. B_m can then be determined from (41) and from the equation for the demagnetization curve of a rigid magnet:

$$B_m = B_{0m} + B_R = B_{0w} + B_R = B_w + B_R \quad . \tag{42}$$

Substitution of this expression into (41) yields A_m:

$$A_m = B_w A_w / (B_w + B_R) = A_w / (1 + B_R / B_w) \tag{43}$$

To find the cladding thickness necessary for flux confinement, we take our zero potential to be at the left pole piece in Fig. 8. For any point,C, on the outer surface of the cladding to be at zero potential the line integrals of H from A to B and from B to C must be equal and opposite, that is

$$B_w Y_B = -B_{0C} t_B. \tag{44}$$

Since no flux flows radially through the cladding, B_{cm} is zero; and the rigid-magnet demagnetization curve shows that B_{0C} is equal to the coercivity B_{0C} which in turn is equal to $-B_r$. Therefore, from (44) we see that the thickness, t, anywhere must be

$$t = - B_w x / B_{0C} = B_w x / B_R \qquad (45)$$

Again, t is linear in x and a conical surface results, as shown in Fig. 8. Because it is at the same potential as the right end of the supply magnet, the pole piece on the right must also be encased in cladding of maximum thickness.

The actual structure of Neugebauer and Branch employed two tandem chambers with oppositely directed fields, so that cladding of the bases of the high potential pole pieces was unnecessary; a single iron disc served as a common high potential pole piece for the two chambers. (See Fig. 9.)

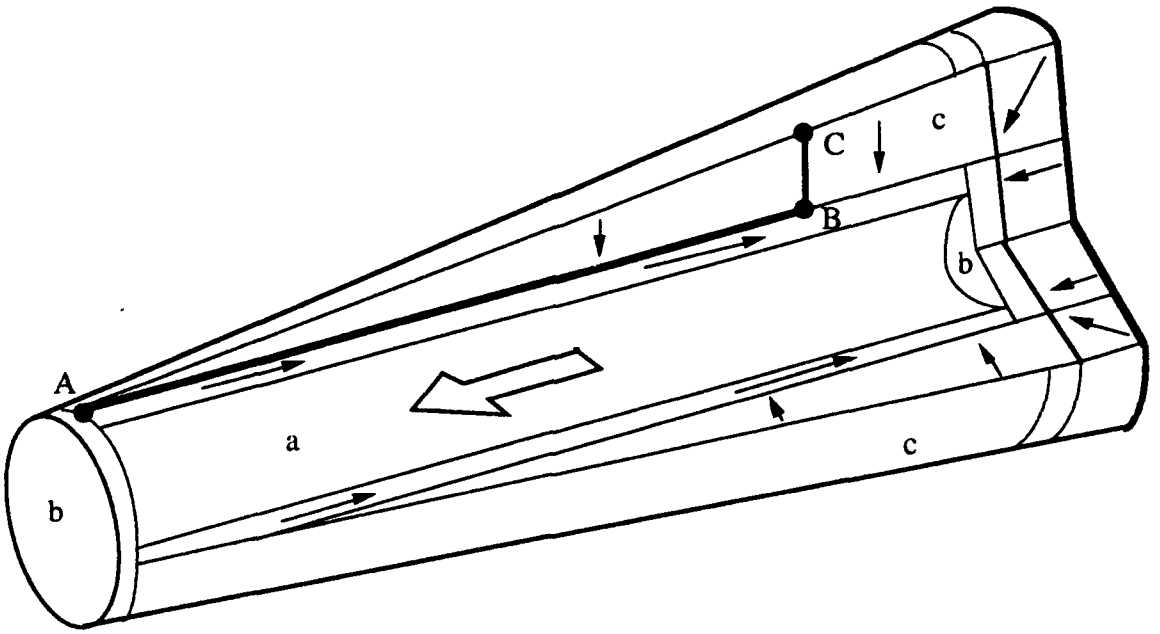

Figure 8. Permanent magnet solenoid of the Neugebauer-Branch type. **a**. Flux supply magnet. **b**. Pole pieces. **c**. Cladding magnets.

A single-chambered structure can be made to be much less bulky than the Neugebauer configuration by taking the plane midway between pole pieces to be at zero potential.[8,9] Then, the cladding is in the form of two conical structures of half the base thickness of the Neugebauer structure. (See Figs. 10 and 11.) The cladding to the left is oriented outward and that to the right inward. Figure 11 compares the two structures and the corresponding potential differences between the inner and outer surfaces of the cladding. In the Neugebauer structure, shift of zero potential from chamber end to chamber center would result in an approximately 60 percent reduction in mass.

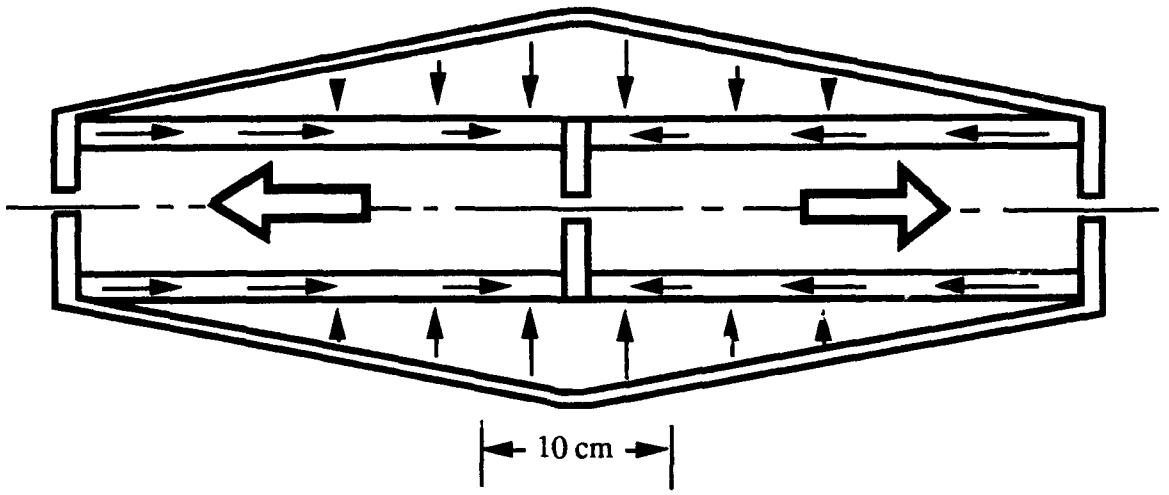

Figure 9. Tandem chamber klystron magnet by Neugebauer.

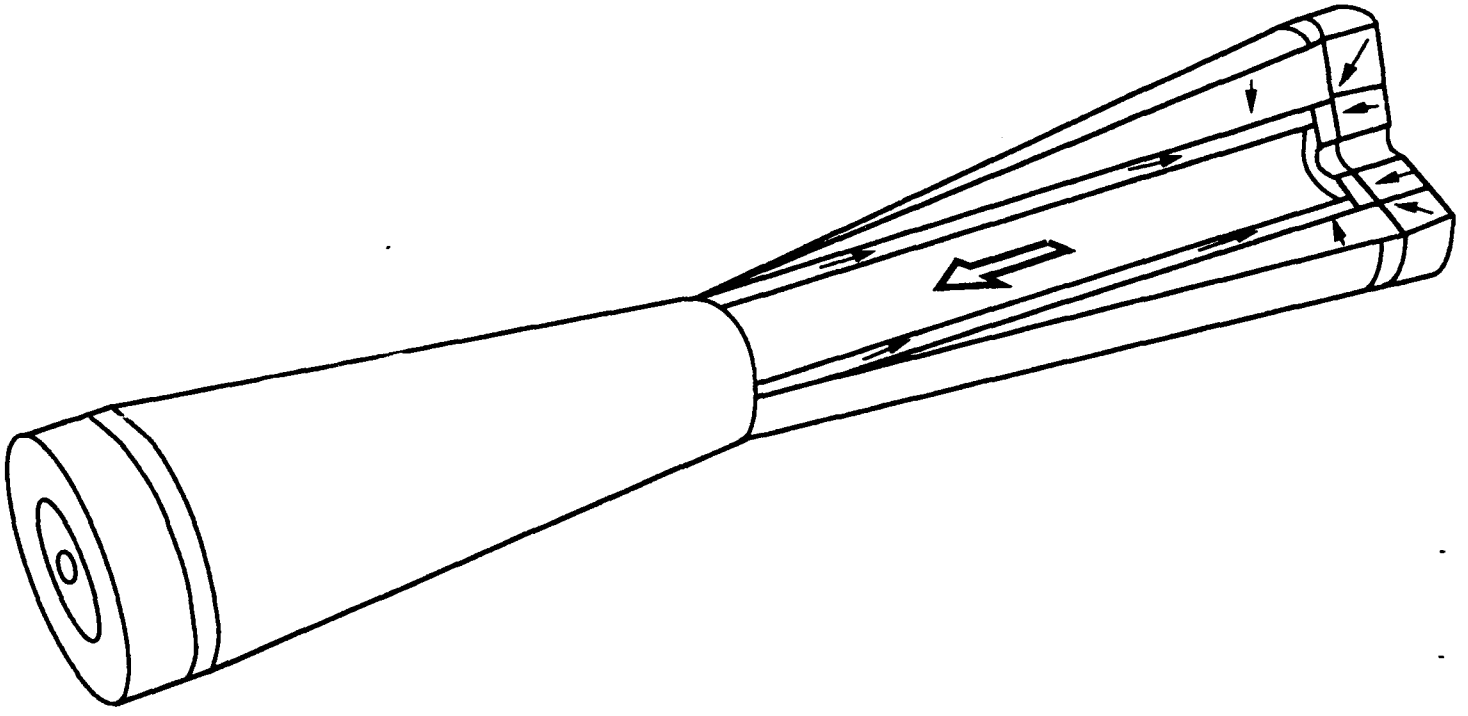

Figure 10. Because the zero potential reference has been moved to the middle from the end, the ETDL structure pictured here has less than half the mass of the Neugebauer design of Fig. 8. Solenoidal fields up to 0.5 Teslas are easily produced in this manner, in a structure much lighter than an equivalent electric solenoid and its power supply.[7-9]

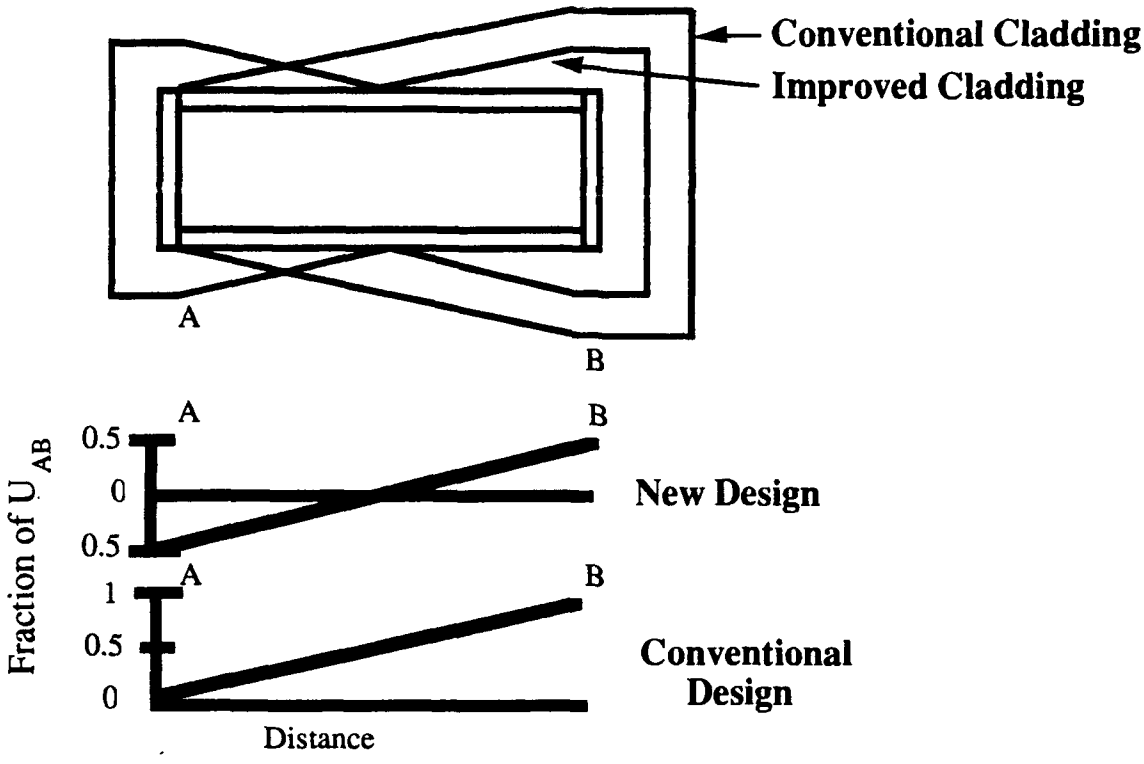

Figure 11. Comparison of Neugebauer and ETDL structures.

Figure 12 shows a computer plot of the magnetic flux produced by the improved structure. There is some leakage due to imperfect cladding at the ends of the structure. Figure 13a shows the axial field as a function of distance from a chamber end. Figure 13b shows the much improved field uniformity obtained after a simple correction to the cladding slope is made. The correction consists of an increase of cladding thickness Δt according to the formula:

$$\Delta t = (H_D - H_A)\, t / H_A \qquad (46)$$

where H_D is the desired field and H_A is the actual field.

The unviability of conventional magnetic materials for construction of such clad structures is illustrated in Figure 14, which shows the demagnetization curves for $SmCo_5$ and for alnico. The flux density for the former is seen to be much higher when used as a source in a permanent-magnet solenoid. Even more important is the disparity in magnetic field in cladding magnets, as evidenced by the tenfold superiority in coercivity of the $SmCo_5$. Since cladding thickness is inversely proportional to the coercivity, the bulk of cladding in an alnico structure would be about one hundred times that in a $SmCo_5$ configuration. Further, such great cladding thicknesses result in unacceptable backstreaming of flux through the cladding normal to its magnetization.

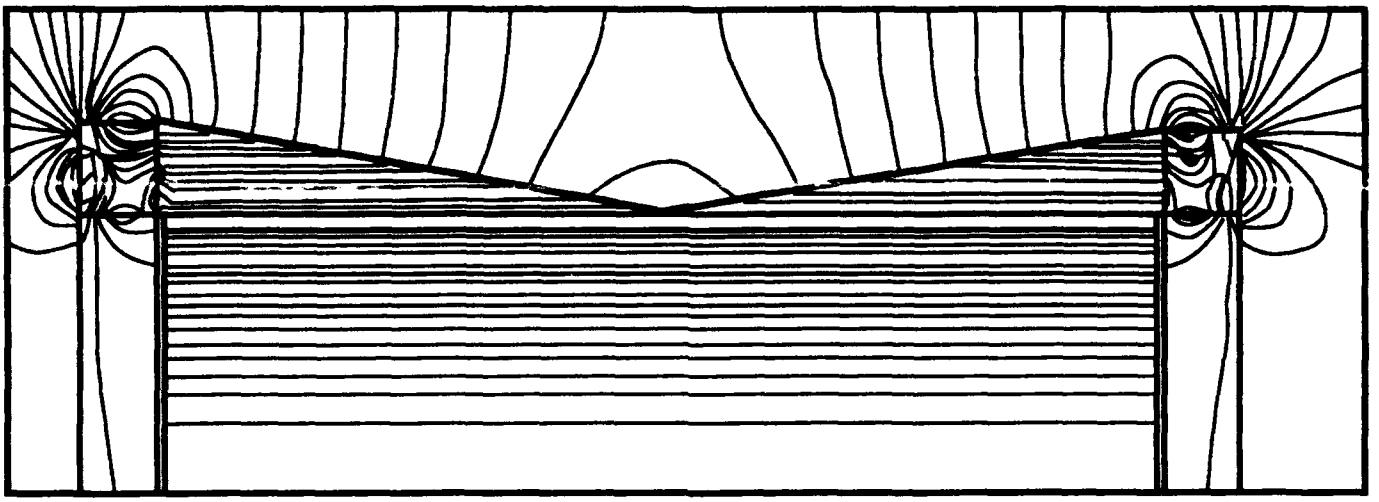

Figure 12. Flux plot of magnetic field produced by the permanent-magnet solenoid of Fig. 10. Note the great uniformity over the working space. Apparent flux crowding towards the periphery is because each line represents a unit of flux in an annular ring of given thickness. Actual leakage is only a few percent and is due to imperfect cladding at the corners.[8] This is easily remedied by a slight increase in slope of the cladding cone over that prescribed by Eq. (45).

There are many useful variants of the permanent magnet solenoid. For example, the internal field need not be constant but can be varied along the axis by appropriate adjustments in the supply magnet and cladding thicknesses.[8,10] As an example, if the field is to increase linearly with progression along the axis, the cross-sectional area of the supply magnet must also increase linearly while the cladding thickness is parabolic. In such a structure, the most efficient placement of zero potential is at the magnetic center **C** of the configuration, that is, where the line integral of the field along the axis over the length of the chamber attains half its value viz

$$\int_0^C \vec{H}\cdot d\vec{l} = \int_C^L \vec{H}\cdot d\vec{l} \qquad (47)$$

where 0 and L are the ends of the working space. Clearly **C** lies on the high field side of the geometric center and the cladding is concave on the high field side and convex on the low field side.

The structural variations necessary to obtain the desired fields can be effected parametrically as well as geometrically, that is, material properties of the magnets can be varied rather than their dimensions.[8-10] This procedure is not as efficient with regard to

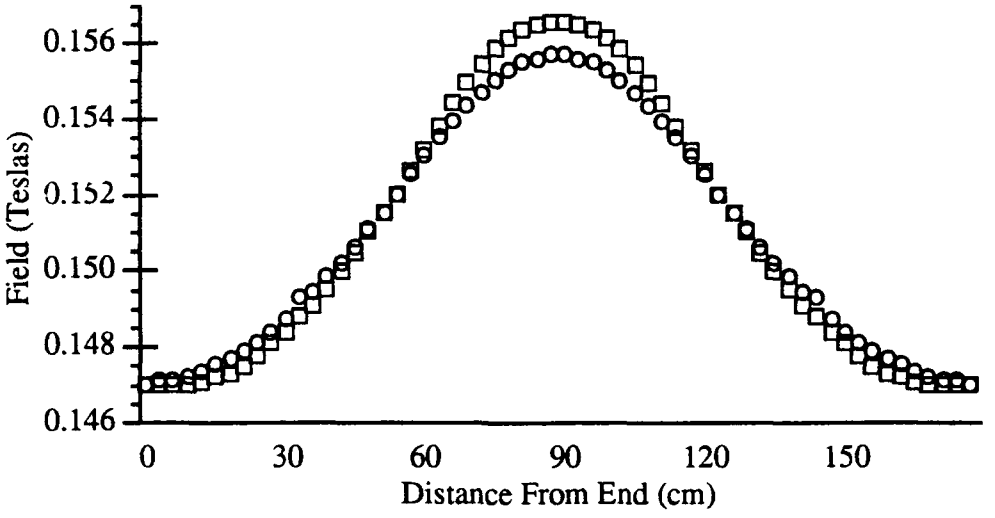

Figure 13a. Magnetic field profile along the axis of the cylindrical structure. The ○ are the on-axis fields and the □ are 20 cm off the axis of rotation.

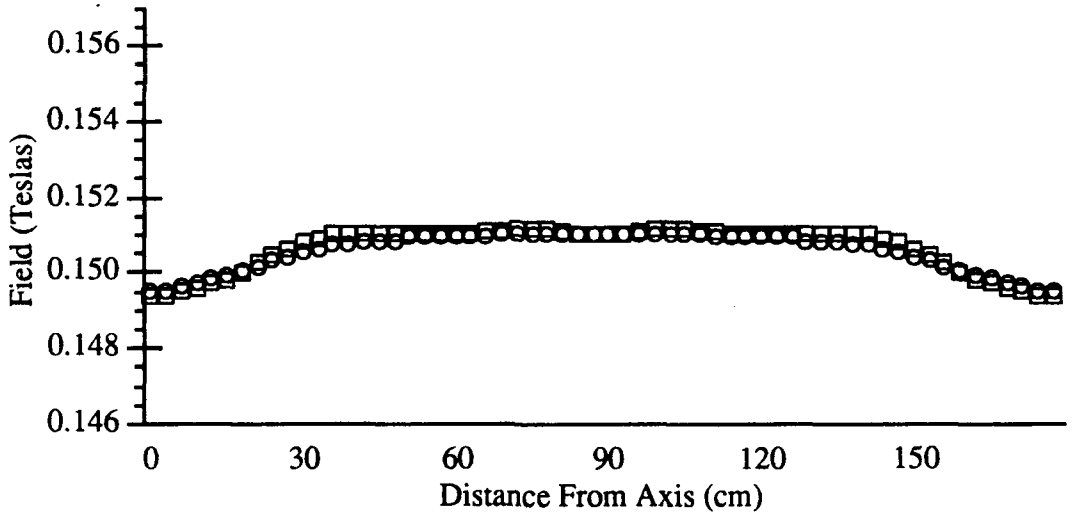

Figure 13b. Magnetic field profile along the axis of the cylindrical structure with quasi-optimized cladding magnets. The ○ are the on-axis fields and the □ are 20 cm off the axis of rotation.

structural weight and bulk because the uniform cladding thickness must be that of the maximum thickness in the geometric structure. On the other hand, in the parametric configuration, the ring magnets are all of the same dimensions and are easier to manufacture. A prototype constructed at ETDL is a hybrid in which the cladding is varied

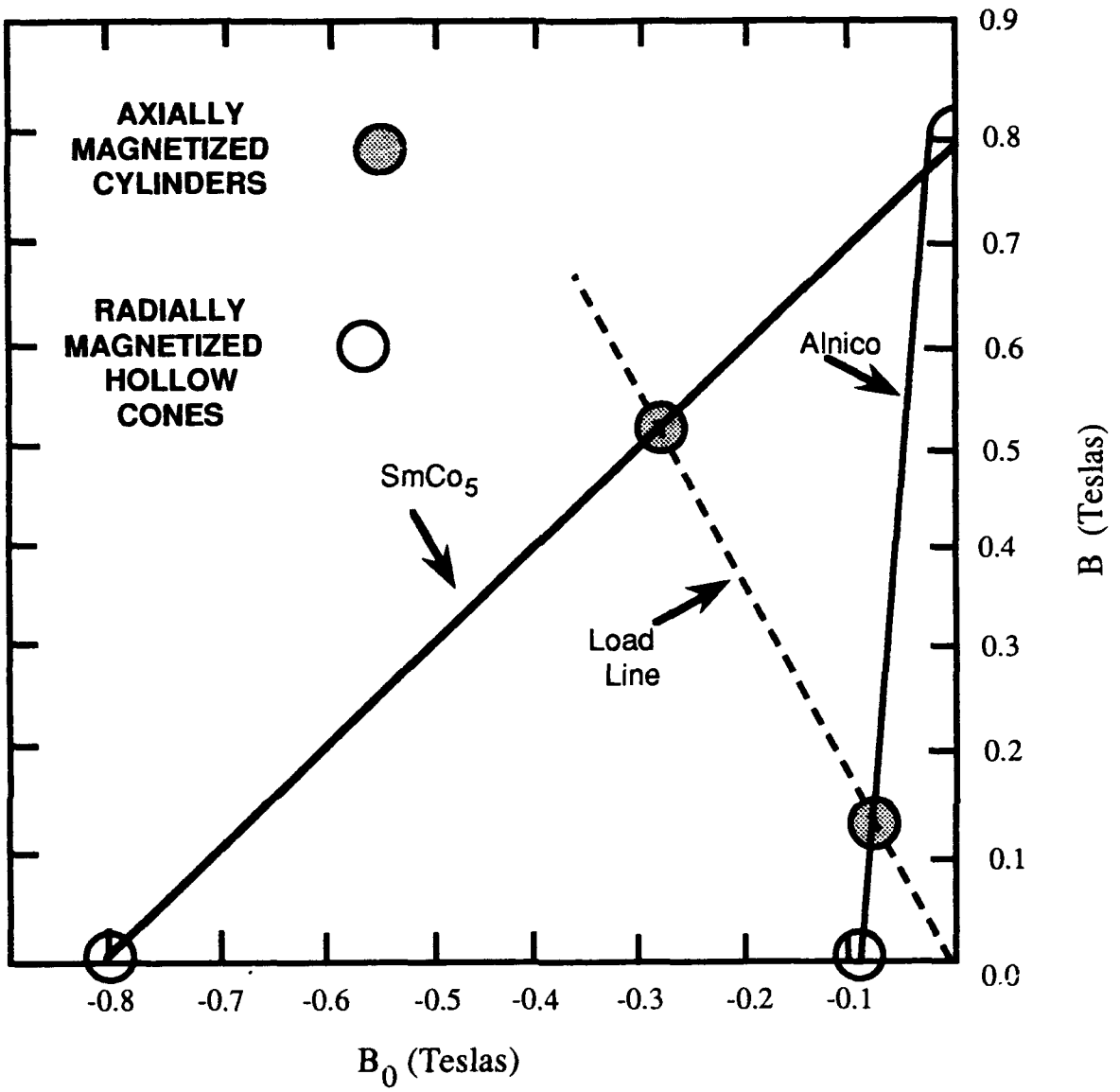

Fig. 14. Demagnetization curves and operating points for the magnets in a solenoidal field source.

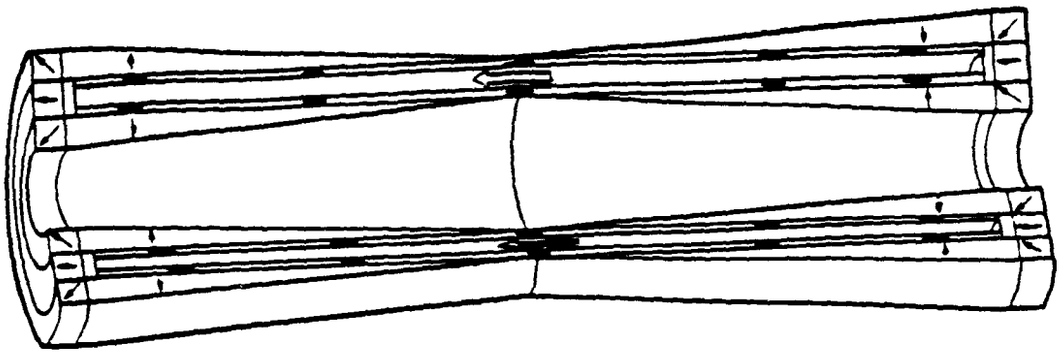

Figure 15. Permanent magnet annular field source

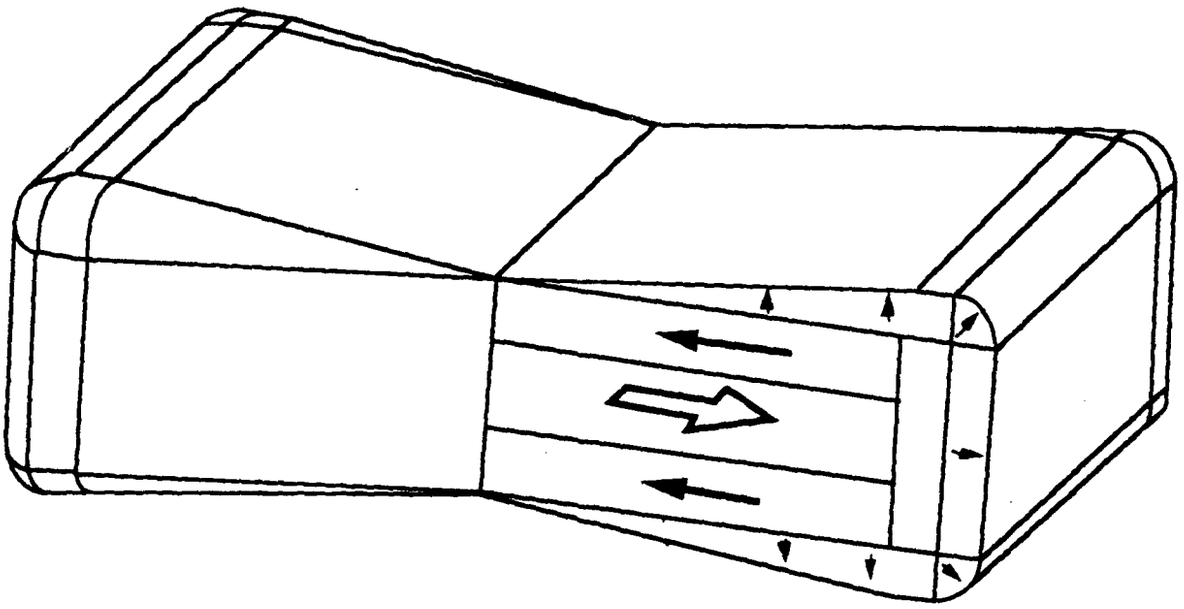

Figure 16. Clad rectangular field source

geometrically and the supply magnets parametrically. This was done to save weight in the bulky cladding magnets and to facilitate manufacture of the much thinner supply magnets whose fragile walls make a geometric taper impracticable.

The outlined principles can be applied to other field configurations such as in the cylindrical structure of Fig. 15 in which the field is confined to an annular ring by the

placement of cladding in the inner boundary of the working space as well as on the outer.[11] In this arrangement, the supply magnets can be at the outer boundary of the working space, on both the inner and outer boundaries or on the inner boundary. The last of these is the most efficient with regard to the total bulk of the structure provided that the inner hollow is spacious enough to accommodate both the inner cladding and all of the supply magnet. Cross sections need not be cylindrical. Figure 16 shows a rectangular array with cladding. Clad structures with fields normal to the axis are also possible as in Fig. 17.[9] Such configurations are potentially useful for Magnetic Resonance Imaging (MRI) which at present employs costly and cumbersome superconducting electromagnets.

Finally, some cross-sections of such devices can be rotated about appropriate axes to form structures with radial fields such as those of Fig. 18.

All clad structures lose some of their field uniformity if access holes are drilled

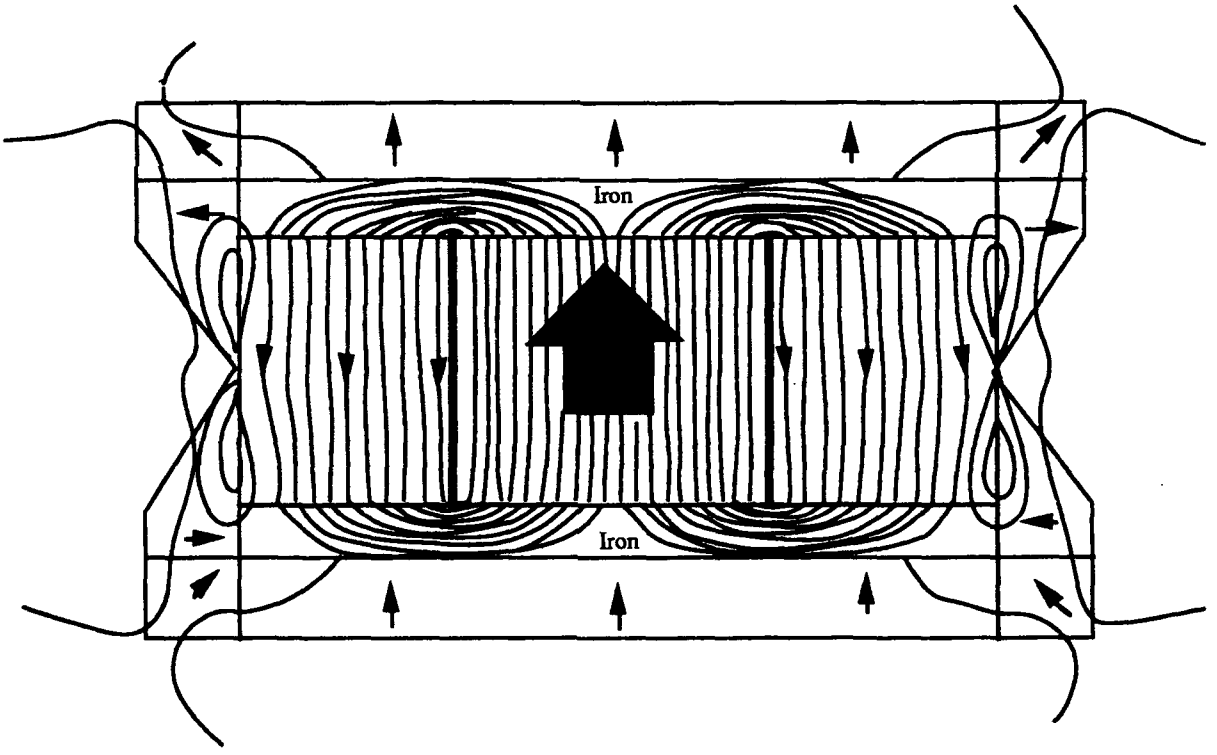

Figure 17. Transverse fields source for a long rectangular cavity. The large arrow is the field in the cavity. The medium sized arrows are the orientations of the permanent magnets and the small arrows denote the directions of the flux lines.

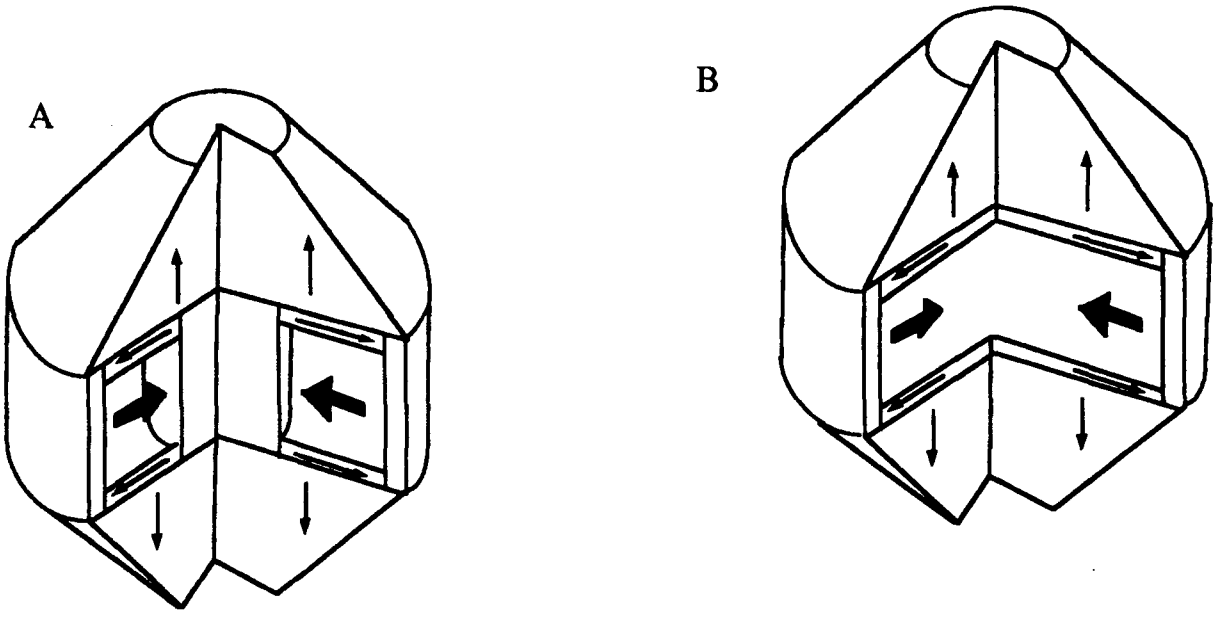

Figure 18. Radial field flux source, A , with central iron flux guide. B, without central iron post. The field in B becomes distorted near the structural axis.

into their interior cavities. Such holes can often be made to be axially symmetric so that the field distortions are also axially symmetric and can be at least partially compensated for by methods similar to that employed in the compensation illustrated in Fig. 13.

If only one hole is needed in a structure that has its zero of potential at an end, it is usually better to drill the hole at that end since then no penetration of a cladding magnet is necessary and less field distortion results.

Structures Composed Entirely of Rigid Permanent Magnet Materials

Structures that employ pre-REPM magnets are used, for the most part, with iron flux guides or yokes to shape and intensify the field in a working space. For many working-space geometries, it would be better to arrange magnetic poles so that maximum field is produced where it is wanted. Of course, there are no free magnetic poles; they are always accompanied by a like number of opposite poles of equal strength. It is the goal of yokeless magnet design to place the component magnets so that their poles are as effectively placed as possible to produce the desired field where needed and the opposite poles are more remotely placed or negated. Because the optimal arrays often entail very strong demagnetizing fields, the art of yokeless magnet design has very limited applicability with the older magnets of low coercive force.

Simple all-magnet structures that produce extraordinarily high fields can be obtained through considerations of symmetry and a very useful theorem.[12,13] The latter

states that *if a dipole is rotated about one of its axes normal to the dipolar axis through a given angle , the field it produces is everywhere rotated by the same angle in the opposite sense*. As an example of this procedure, we consider a cylindrical cavity of infinite length in which it is desired to generate a uniform field transverse to the principal axis. If this is to be accomplished with permanent magnet material in the form of a circumscribed cylindrical shell, it is clear that the orientation of magnetization must have reflection symmetry in the equatorial plane parallel to the desired field direction, as in Fig. 19. By symmetry, the magnetization of the infinitesimal sector, **A**, at the configurational polar line must be oriented radially inward in the direction of the desired field.

If all the other sectors of the annular magnet ring were also pointed radially inward, each would contribute a field, dH_w, at the center of the cavity equal to that of **A** in magnitude, but oriented at an angle of ϕ to that of **A**, where ϕ is the azimuthal angle. Of course, this would result in mutual cancellation of all the dH_w's. According to theorem, if the orientation of each segment is now changed by $-\phi$, the fields of the individual segments would all be in the same direction everywhere and hence would add without cancellation. Therefore, the prescription of the theorem is that the orientation of magnetization γ be in the direction

$$\gamma = 2\,\phi\,. \tag{48}$$

The magnetic field in the cavity can then be found either by determination of the surface, σ_S , and volume, σ_V , pole densities arising from the magnetization $\vec{M}_0$ and insertion of the results into Coulomb's law, or by application of Maxwell's equations to the boundaries of the magnetic material. The pole densities are given by

$$\sigma_S = \hat{n} \cdot \vec{M}_0 \tag{49}$$

$$\sigma_V = -\nabla \cdot \vec{M}_0 \tag{50}$$

where $\hat{n}$ is the unit vector normal to the surface under consideration. The resulting field in the cavity is uniform and given by

$$B_0 = B_R \ln (R_2 / R_1) \quad . \tag{51}$$

Thus it is seen that there is no limit to the magnetic field that can be obtained in such a structure provided only that the outer radius R_2 be made large enough. Due to the logarithmic dependence of B_0 on R_2 , material bulk quickly becomes prohibitively large with relatively small field increments. Nevertheless, fields of twice the material

remanence should be practicable, namely 2.0 to 2.5 Teslas for the highest energy product materials, e.g., Nd-Fe-B. If, for example, B_R = 1.2 Teslas, the working space is 2.5 cm in diameter and the outer structural diameter is 15 cm., the internal field will be given by

$$B_{0W} = 1.2 \ln (15/2.5) = 2.1 \text{ Teslas} \tag{52}$$

which is an impressive field to be generated in so large a working space by a structure that can be packed into a cylinder 15 cm in diameter and which confines its field completely to its interior.

Ease of manufacture can be facilitated by approximation of the cylindrical boundaries with circumscribed polygons as in Fig. 20.[1] If this is done, the expression for the field becomes

$$B_{0W} = B_R\left[\cos\left(\frac{2\pi}{N}\right)\ln(R_2 / R_1)\right] \tag{53}$$

where N is the number of sides of the polygons. Even polygons with as few as eight sides still result in a field nearly 90% of that obtained with ideal circular cylindrical surfaces.

Structures of this type are useful for any application in which high transverse fields

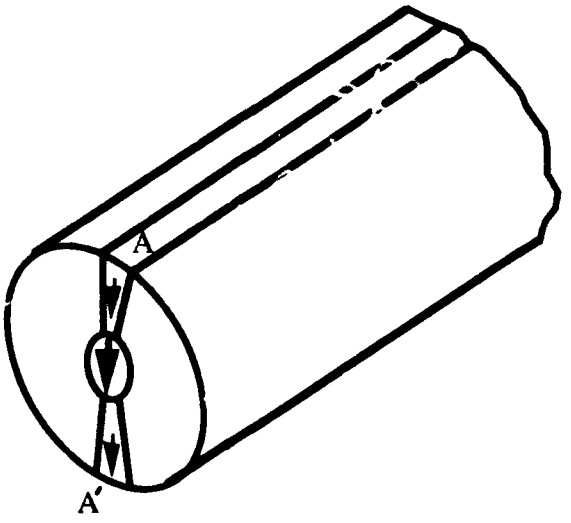

Figure 19. If a cylindrical dipolar source is to produce a uniform field in a cylindrical cavity as shown above, it is clear from symmetry that the infinitesimal elements A and A' must be oriented as shown.

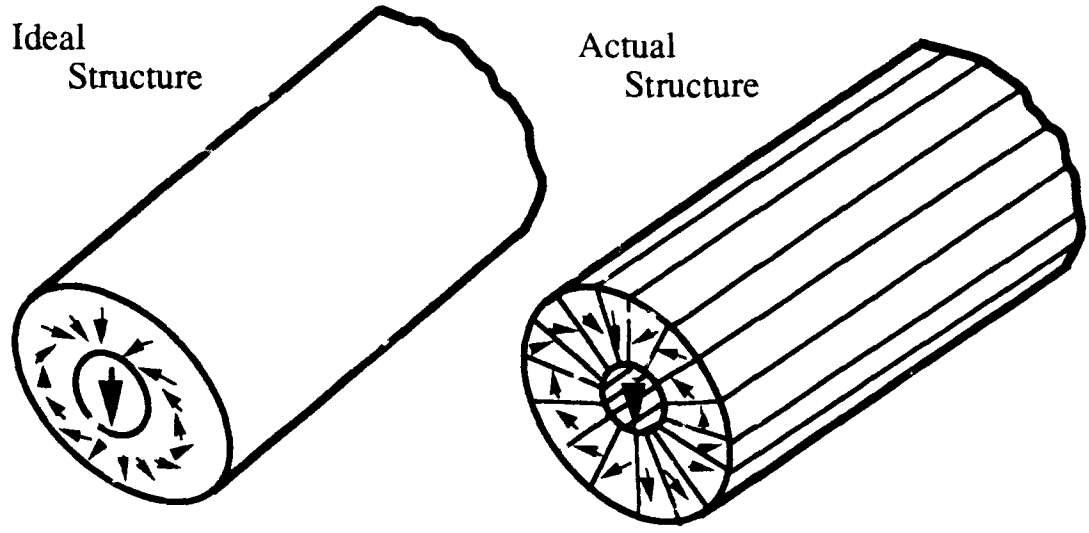

Figure 20. Structure that produces the field specified in Figure 19 as derived from symmetry and the dipolar rotation theorem.

are required in elongated cavities as in nuclear magnetic resonance imagers, biasing fields in electronic filters and general utility laboratory magnets. Cross-sectional slices of the structures can be used as segments of wigglers and undulators of free electron lasers to provide higher fields with less bulk and mass than is possible with more conventional structures (Fig. 21).[14,15]

The cylindrical structures can also be made to be mechanically adjustable.[16] This is done by fabrication of the magnet in two pieces with one nestled inside the other as in Fig. 22. Then the field within the central cavity will be the vector sum of the fields produced by the individual rings. If the rings each produce one half the field individually and are rotated with respect to each other by an angle θ, the magnitude of the field within the cavity is just

$$B_0(\theta) = B_0(0) \cos(\theta / 2) \qquad (54)$$

where $B_0(0)$ is the maximum field, which occurs at zero θ. Thus any field in the range $\pm B_0$ is easily available. For field equality of the individual rings, the radius R_B of the boundary between them must be the geometric mean of the outer and inner radius of the device:

$$R_B = \sqrt{R_1 R_2} \qquad . \qquad (55)$$

Fields of higher multipole value than dipole can also be generated by an appropriately faster change in variation of orientation, γ, with ϕ, so that

$$\gamma = n\,\phi$$

where n is 2 for a dipole, 4 for a quadrupole, and so on.

To make a ring of this type it is not necessary to make the many pieces with different orientations individually. For example, in the manufacture of a dipolar source, it is only necessary to orient a ring in a single unidirectional field, as in Fig. 23a. The ring is then cut into as many sectors as the desired approximation to a perfect ring demands. The pieces are interchanged according to the prescription $\phi \leftrightarrows -\phi$ as shown in Fig. 23b and glued together to form the desired structure in Fig. 23c. This is possible because every possible orientation of magnetization with respect to the local radius is contained in the structure of Fig. 23a. They need only be reassembled to yield the dipolar source of Fig. 23c.

A similar procedure can be used to make higher pole sources, but then **n** structures such as that of Fig. 23a are required to yield the **n** of the desired n-poled arrays. The sequence of assembly of a quadrupolar source is shown in Fig. 24.

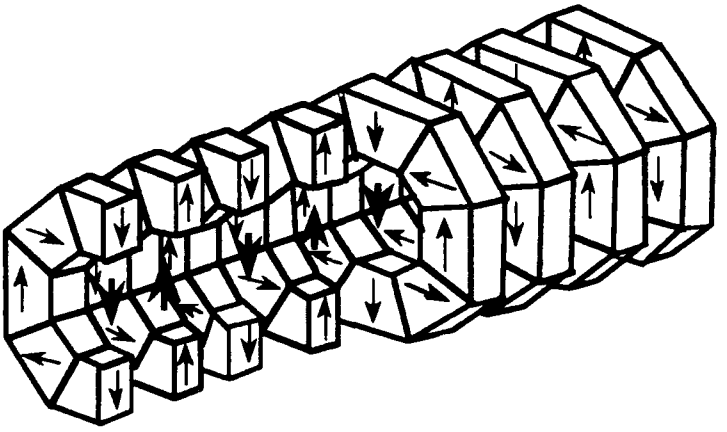

Figure 21. Wiggler made from slices of octagonal cylindrical transverse field sources.

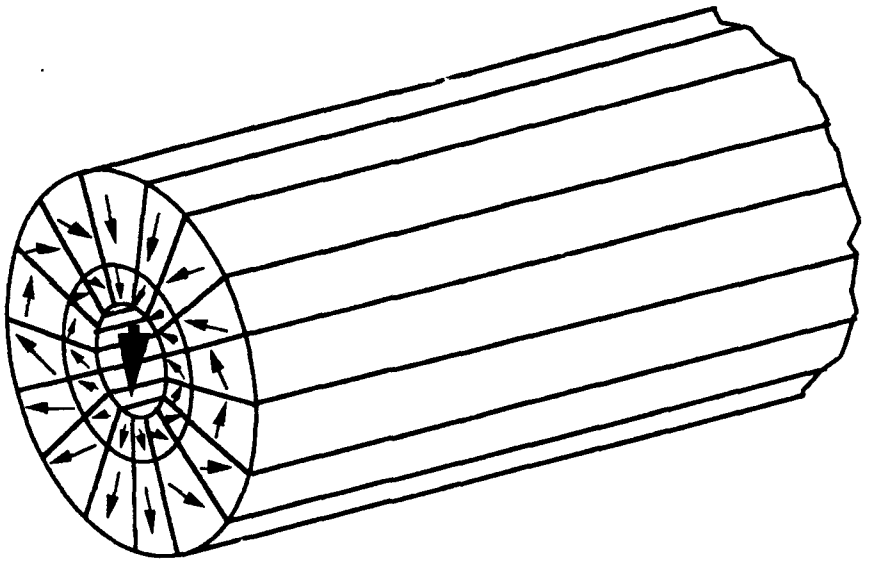

Figure 22. Adjustable circular-cylindrical transverse field source.

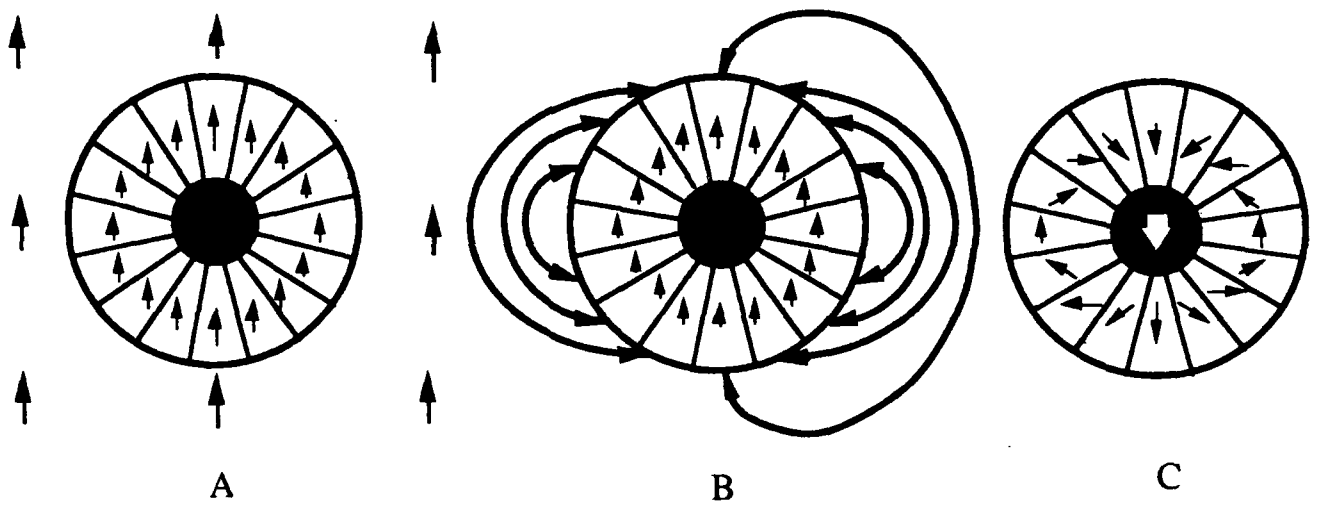

Figure 23. Construction of circular-cylindrical transverse field source. A. Structure is magnetically aligned (small arrows) in a uniform magnetic field (big arrows) and sliced into segments (dotted lines). B. Pieces are interchanged as shown and bonded to form the finished structure C.

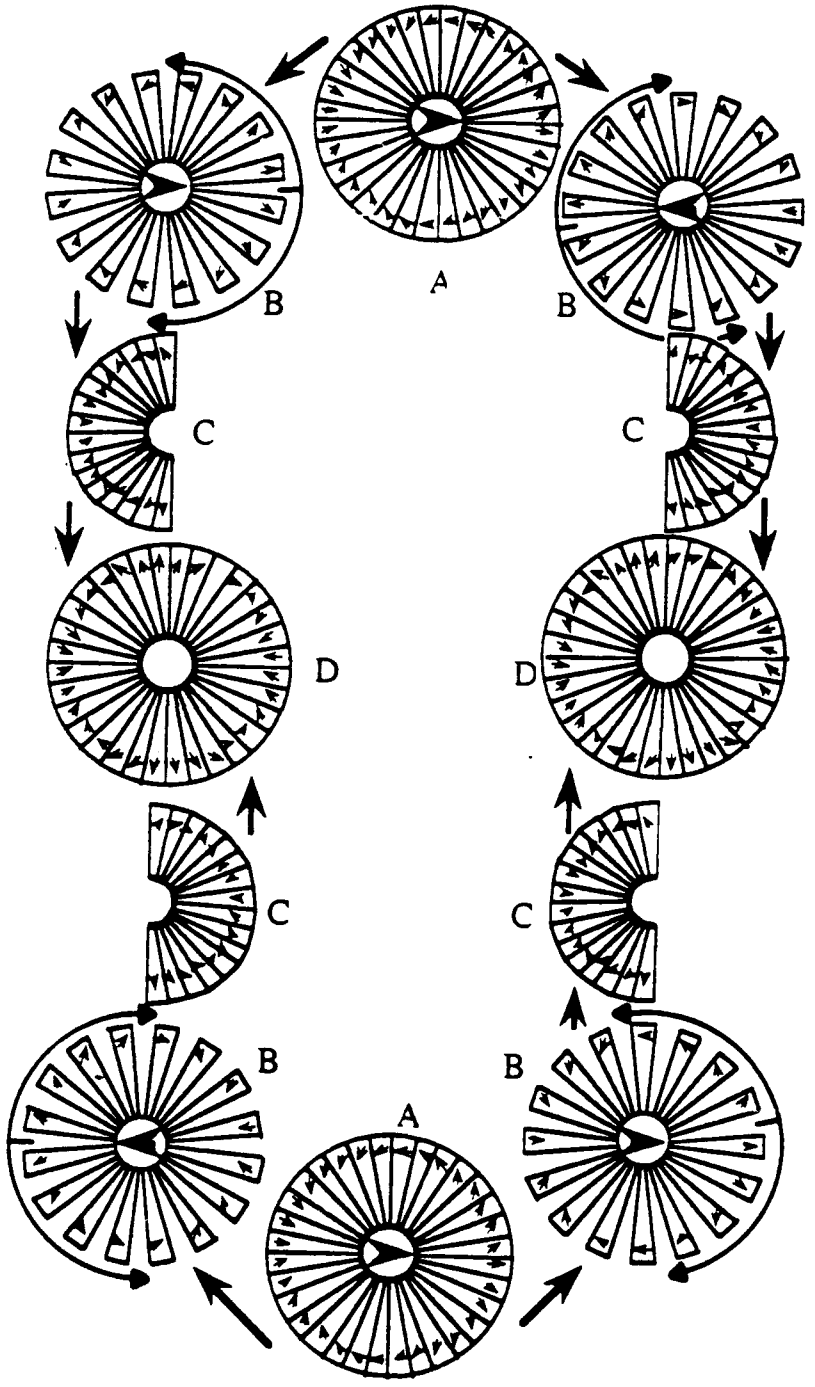

Figure 24. Formation of two quadrupole sources from two dipole sources. A. Start with two dipolar structures A. B. Separate every other segment from adjacent segments to form two new structures for each original structure. C. Compress structures B in direction of circular arrows to form structures C. D. Assemble structures C to form structures D.

Flux Confinement to Polygonal Cavities

It is often desirable to produce a strong transverse magnetic field in a cylindrical cavity of equilateral polygonal cross section. It is sometimes further required that the magnetic field be completely confined to within the outer boundaries of the structure with said boundaries being parallel and similar to the cavity boundaries. The latter requirement is to ensure the possibility of successive nesting of similar structures within each other to take advantage of the additive property of such fields to produce a large interior field equal to the sum of the components. Because of its usefulness in MRI,[17,22] a square cross section due to Abele will be considered as an example of the method of determination of the structure.

We begin with a consideration of the top segment of the square magnet. It is of trapezoidal cross section with 45 degree base angles. Because of square symmetry, only one half of it need be considered. For simplicity, it is desirable to have fields, magnetization and flux density constant over any of the segments into which the half trapezoid is to be divided. It is not possible to accomplish this together with flux confinement and generation of the desired field with a single piece. Accordingly, to attempt to fulfill all the requirements, we divide the segment into two triangular pieces 1 and 2 as shown in Fig. 25. Since it is clear that the orientation of the magnetization in segment 1 should be in the direction of the desired flux density B_W, we need only determine the thickness t and the orientation of the magnetization in segment 2 that will fulfill the requirements:

(1) That there be no flux exterior to the structure.

(2) That the specified uniform flux density, B_W , be generated in the interior cavity.

(3) That the exterior boundary of the structure be a square.

The first condition applied to the circuital form of Ampere's law dictates that

$$B_{01}y + B_{02y}(t-y) + B_W r_1 = 0 \tag{56}$$

or if paths of integration **ab** or **cd** of Fig. 25 are chosen

$$B_{01}t = B_{02y}t = -B_W r_1 \tag{57}$$

so that

$$B_{01} = B_{02y} \tag{58}$$

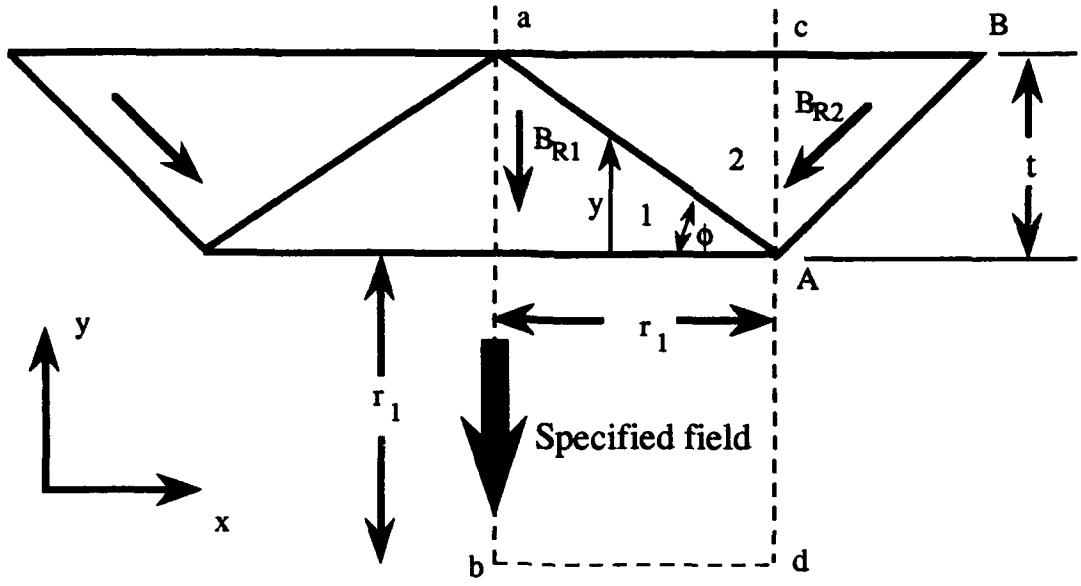

Figure 25. Determination of configuration of upper segment A square dipolar field source.

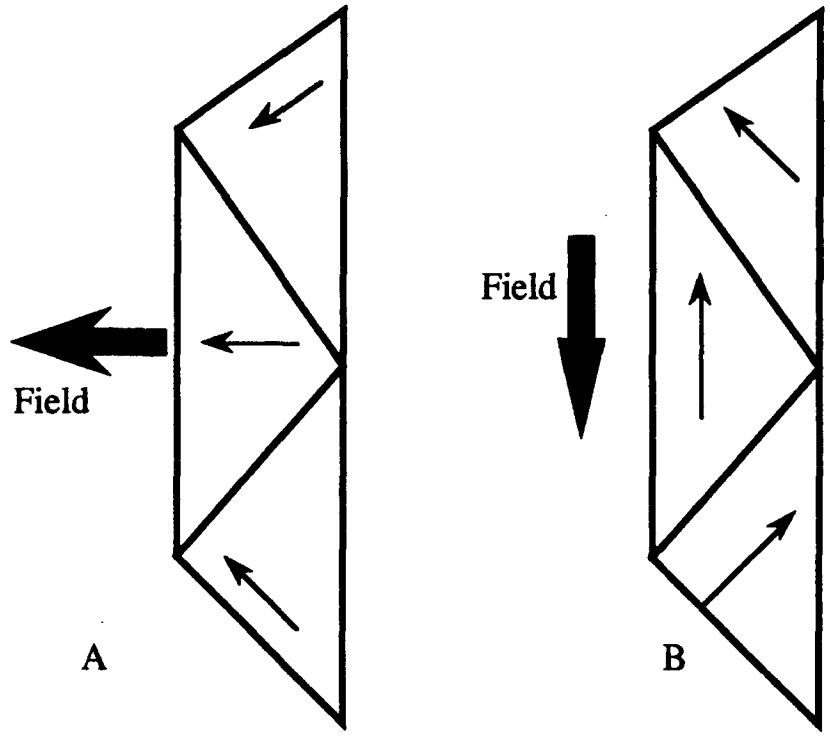

Figure 26. **A.** Side segment of square if relative magnetic orientation were that of Fig. 25. **B.** After -90° rotation of all magnetizations.

The second condition applied to Gauss's law at the cavity boundary yields

$$B_1 = B_W \quad . \tag{59}$$

And since

$$B_1 = B_{01} + B_R \tag{60}$$

(59) becomes

$$B_{01} = B_W - B_R \tag{61}$$

and insertion of (61) into (57) determines t viz

$$t = \frac{-B_W r_1}{B_W - B_R} = -\frac{r}{B_W / B_R - 1} r_1 \tag{62}$$

$$t = \frac{r r_1}{1 - r} \tag{63}$$

where $r = B_W / B_R$, that is, the fraction of the remanence flux density of the magnet that is manifested as useful flux density in the cavity. The fraction **r** cannot be chosen arbitrarily if the outer boundary is to be a square. To demonstrate this, we apply Ampere's and Gauss's laws to the outer surface. For **B** and **H** to be zero everywhere exterior to the outer boundary, these laws require that $B_{02X} = 0$ and $B_{2Y} = 0$ so that B_{02} and B_2 must be mutually perpendicular and respectively normal and parallel to said boundary and since $\vec{B}_{02} + \vec{B}_R = \vec{B}_2$

$$(B_{02})^2 + (B_2)^2 = B_R^2 \quad . \tag{64}$$

Since the outer boundary is a square with its sides parallel to those of the inner boundary, application of Gauss's law at the boundary (1,2) yields

$$B_2 \sin \phi = B_1 \cos \phi \tag{65}$$

$$B_2 = B_1 \operatorname{ctn} \phi \tag{66}$$

where ϕ is the angle between (1,2) and the inner boundary.

If we insert (65) and (66) into (64), we get

$$B_1^2 \mathrm{ctn}^2\phi + B_{02}^2 = B_{R2}^2 \tag{67}$$

but

$$B_{01} = B_{02y} = B_{02}\,,\ \mathrm{ctn}\,\phi = r_1 / t,\ B_1 = B_W \text{ and } B_0^1 = B_W r_1 / t \tag{68}$$

so that (67) becomes

$$2B_W^2 (r_1 / t)^2 = B_{R2}^2 \tag{69}$$

$$2(r r_1 / t)^2 = 1 \tag{70}$$

$$\sqrt{2}\, r r_1 = 1 \tag{71}$$

From (63) and (70) we get

$$\sqrt{2}(1 - r) = 1$$

$$r = \frac{\sqrt{2} - 1}{\sqrt{2}} = 0.293 \tag{72}$$

If (72) is inserted into (70) we obtain the ratio of r_1 to t;

$$\frac{r_1}{t} = \frac{0.707}{0.293} = 2.41 \tag{73}$$

Because from (64), (68) and (69) we have that $B_{02} = B_2$. The angle α between $\vec{B}_{R2}$ and $\vec{B}_2$ is

$$\alpha = \tan^{-1} \frac{B_{02}}{B_2} = \tan^{-1} 1 = 45°$$

so that the direction of $\vec{B}_{R2}$ is parallel to the boundary **AB** of Fig. 25. By symmetry, the directions of magnetization in the side forming the bottom of the configuration are just the inverse mirror images of those just formed for the top side. The magnetization orientations in the other two sides are found by the dipolar rotation theorem. If the side shown in Fig. 26 had its magnetization vectors arranged relative to its sides as in the top side, the resulting field would point to the left as in Fig. 26A. To have the field re-enforce that of the top side it would have to be rotated 90° to make it point straight down as in Fig. 26B. The theorem tells us that for this to be accomplished, the magnetization vectors must all be rotated -90° to form the configuration shown in Fig. 26B and Fig. 27. A permanent magnet material of remanence 1.0 Teslas produces a flux density of

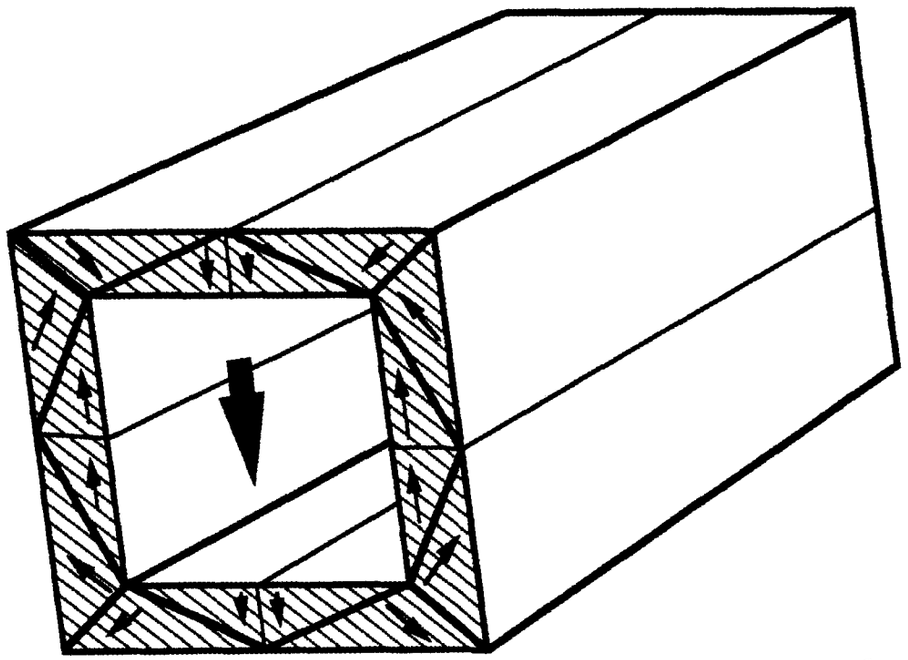

Figure 27. Square dipolar field source. Large arrow shows field in cavity. Small arrows show orientations of constituent magnets.

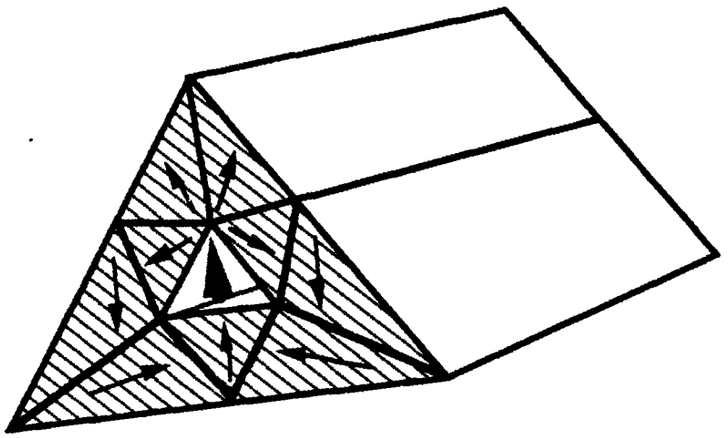

Figure 28. Triangular dipolar field source. Large arrow shows field in cavity. Small arrows show orientations of constituent magnets.

0.293 Teslas and there is no limit to the intensity that can be attained by successive circumscription of similar structures so that the total flux density is 0.293 n Teslas where n is the number of layers used.

Such square structures are particularly useful as MRI magnets because they can be compensated for small random defects incurred in manufacture and assembly. This is accomplished by the placement of small dipoles at the inner or outer periphery of the structure, usually in the inner corners. The magnet is constructed from sectional slices that are compensated individually. The field that an ideal slice should generate is calculated and then compared with the measured actual field. The nature of the deviation field then determines the magnitudes and directions of the compensating dipoles needed. See references 18-19 for details.

The same procedure can be used to find a triangular structure such as that of Abele[28] which fills the same requirements as those specified for the square structure (Fig. 28). Table 3 compares the triangular, square, and circular configurations with regard to structural parameters. The triangular structure produces a higher field with a single layer than does the square. The circular structure produces a higher field than either with the same amount of magnetic material but requires more pieces for a near approximation (99%) to its theoretical performance. Therefore, if simplicity of manufacture is the prime consideration, the triangular section is best, but it is the worst in field strength produced for a given quantity of magnetic material. The circle is best in the latter regard but, as noted, is the most complex. The square is intermediate and can be easily dipole-compensated for structural defects. The octagonal approximation to the circle is simple and produces a strong field but does not afford total flux confinement.

Uniform fields can be provided in cylindrical cavities of any cross-section. The shape need not be symmetrical or even externally convex. The details of the generation of such fields which are beyond the scope of this review can be found in references 20 - 22.

If the required fields are less than about half the remanence, compact sources for fields in axially finite cavities can be made from sections cut from any of the basic symmetrical cylindrical structures. The open faces are then clad according to the same principles described in the discussion of permanent magnet solenoids. A clad section of an octagonal source is illustrated in Fig. 29.

Table 3. Design parameters for the structure of Fig. 2. B_0(Teslas) is the field produced in a 1 cm cavity, A_T(cm^2) is the cross-sectional area of the structure, A_M(cm^2) is the cross-sectional area occupied by material, and B_R is the magnetic remanence of 1 Tesla.

Structure	B_0	B_0/B_R	A_T	A_M	B_0/A_T	B_0/A_M
Triangular	5.0	0.50	5.2	3.9	0.96	1.3
Square	2.9	0.29	2.0	1.0	1.5	2.9
Octagonal	3.2	0.32	1.7	0.83	1.9	3.9
Circular	3.5	0.35	1.6	0.78	2.2	4.5

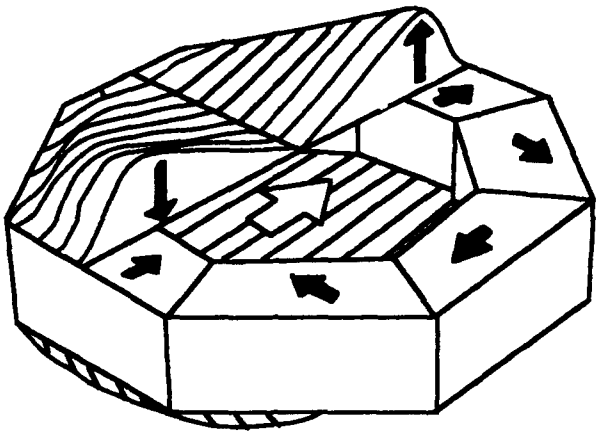

Figure 29. Section of an octagonal pyx. The source of the field is the octagonal ring. The rest of the magnets are cladding to keep the field in the interior (large arrow) confined and uniform.

Three Dimensional Structures

If a thin section of any cylindrical transverse flux source is rotated 180° about its polar axis, a closed chamber is formed in which, of course, there are no end effects as in a finite cylinder and in which the fields are greater than in the corresponding cylinders. For example, the spherical source pictured in Fig. 30a produces a uniform field in its cavity that is four-thirds as great as that in a cylinder with the same inner and outer radius. If B_R is 1.2 Teslas and a flux density of 2.0 Teslas is desired in a cavity 2.5 cm in diameter, the outer diameter of the sphere need be only 10 cm.

The fields produced in the spherical cavities are not only high but remarkably uniform along the axis even when axial tunnels are bored through the poles. Figure 31 shows the field profiles for a sphere with $R_2/R_1 = 2$ and with axial tunnels of varying diameter. It is clear that for tunnels up to one-fourth the internal cavity diameter, the internal field profile is negligibly affected in amplitude and only slightly in uniformity. This suggests great utility for short Faraday rotators or in-tandem periodic structures consisting of strings of spherical elements. The latter is attractive because the field in the tunnels can be made to be nearly the reverse of those in the cavities. Because the square wave field configurations have higher axial field amplitudes than are possible in conventional periodic magnet stacks and because the squareness results in an average field value close to the maximum, the beam focusing ability is much greater than that of the conventional sinusoidal configuration.

A drawback of the spherical structure is that it does not confine magnetic flux completely,[16] but generates a small dipolar field outside of its outer surface. If this field is troublesome for a particular application, it can be easily cancelled by means of a uniformly magnetized shell on the outer surface of the spherical source. It is mounted with its magnetic orientation in opposition to the external field produced by the spherical

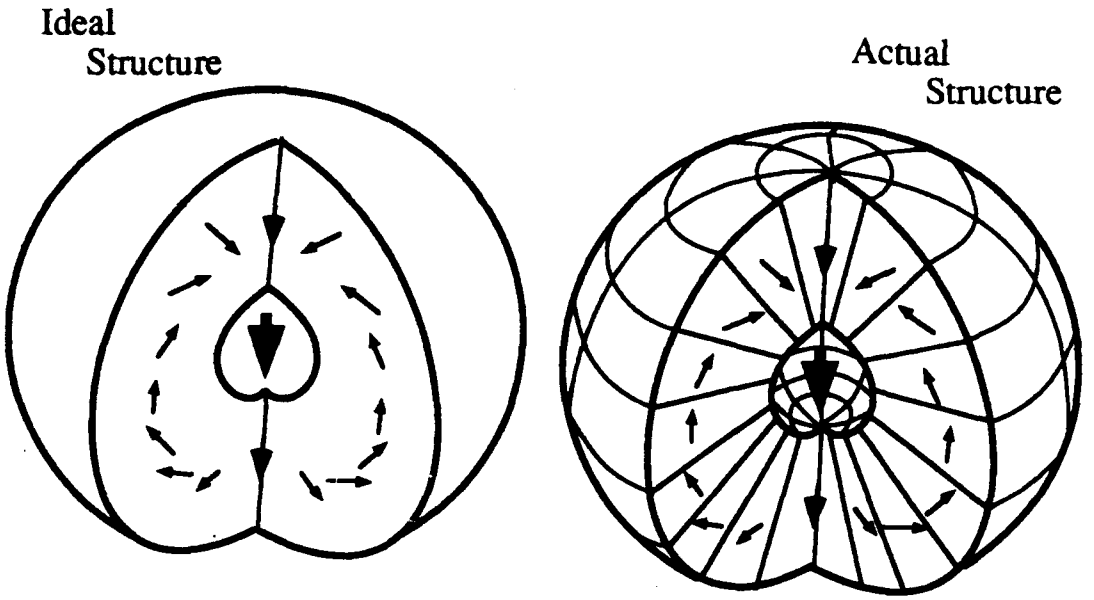

Figure 30. Spherical magnet structure. The field in the central cavity is given by $B_0 = (4\ B_R/3)\ln\ (r_2/r_1)$ where B_R is the magnetic remanence and r_2 and r_1 are the outer and inner radii respectively.

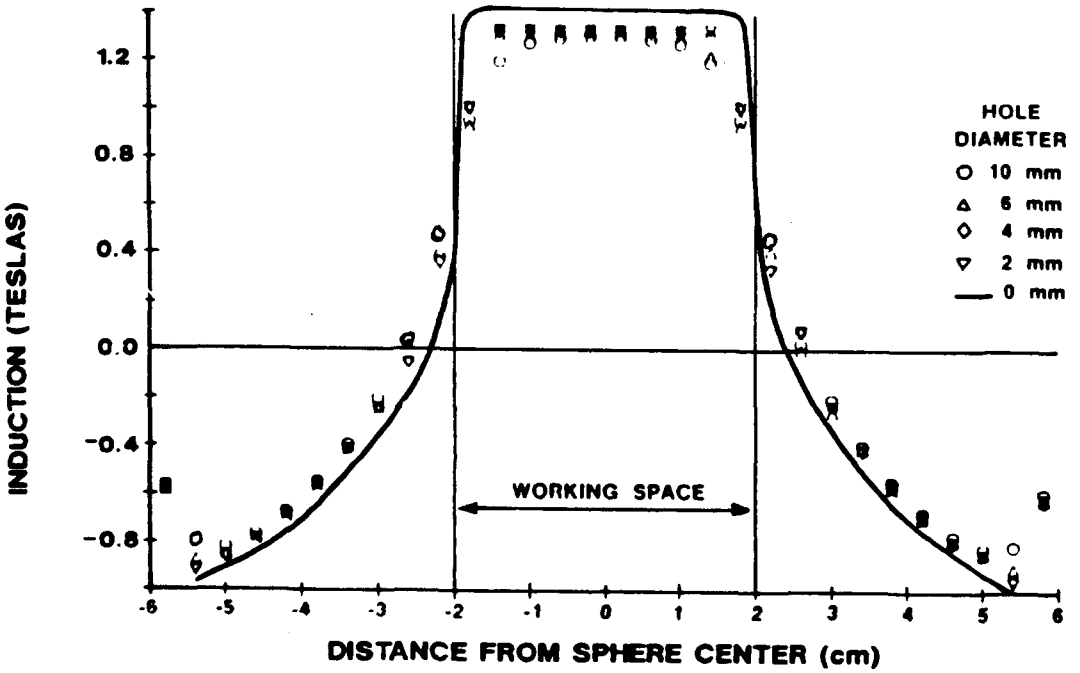

Figure 31. Axial field profile of the magnet structure of Fig. 30. Note the constancy of field in the cavity and also the relative insensitivity to the diameter of the access holes.

source and is given just sufficient magnetic moment to cancel it. Since a uniformly magnetized spherical shell produces no field in its interior, it does not alter the specified field produced by the spherical source in the working space.

Structural Simplification with Magnetic Mirrors

All of these dipolar structures have anti-mirror symmetry in the equatorial plane perpendicular to their polar axes. For this reason, any of them can be cut at the equatorial plane and have either half placed on a high-permeability, high-saturation slab of material such as iron or permalloy to produce the same field in the interior that is produced in the cavity of an entire structure.[23] This works because the anti-mirror image of the half-structure formed in the slab produces the same field in the hemispherical cavity that is produced by the missing half. Such a procedure affords a non-trivial structural simplification since only half as many different magnet segments of complex form need be manufactured for the semi-structure. The working volume is reduced by half, but if the full volume of the working space of the whole structure is needed, it may pay to use a larger half-structure to furnish it. Although then more magnetic material would be used, this drawback is often more than compensated by the increased simplicity afforded by use of only half as many pieces.

The igloo-like structure made of half a sphere and a slab of iron is pictured in Fig. 32. Such a source made of Nd-Fe-B could provide a working flux density of 2 Teslas in a 2.5 cm cavity with an outer diameter of only 9 cm and a weight of 3 kg of permanent magnet material. This is an easily portable source and is potentially a very convenient general-use laboratory magnet. It also has the advantage of an easily accessible interior as lead holes can be drilled through the expendable iron slab rather than through expensive magnet material as in the sphere. This advantage affords greater flexibility with regard to modes of operation as iron slabs with different numbers, positions and sizes of holes would be easily interchangeable. Another advantage of the igloo is that transit through the iron is effected without encounter of field reversals. This is important for some electron-beam and Faraday rotator applications.

If high-temperature superconductors of sufficiently high lower critical field were available above room temperature, it would be practical to further simplify such structures by providing actual rather than anti-mirror images in an axial plane.[23] With various combinations of perfectly diamagnetic (B=0) superconducting mirrors combined with perfectly paramagnetic (B_0=0) iron anti-mirrors, various half-quarter and spherical configurations would be possible. Some examples of such structures are shown in Fig. 33. The simplification afforded by the octant structure is especially impressive as it reduces the practical minimum of seventy-two segments needed to approximate a spherical source to only nine.

A

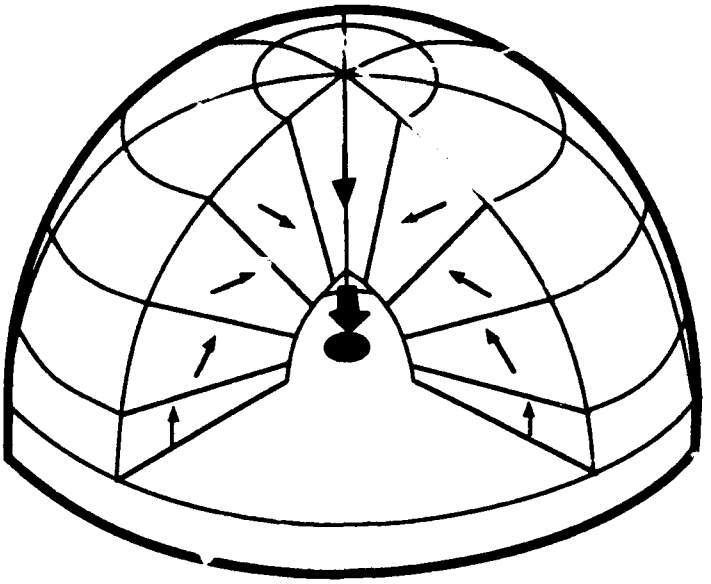

B

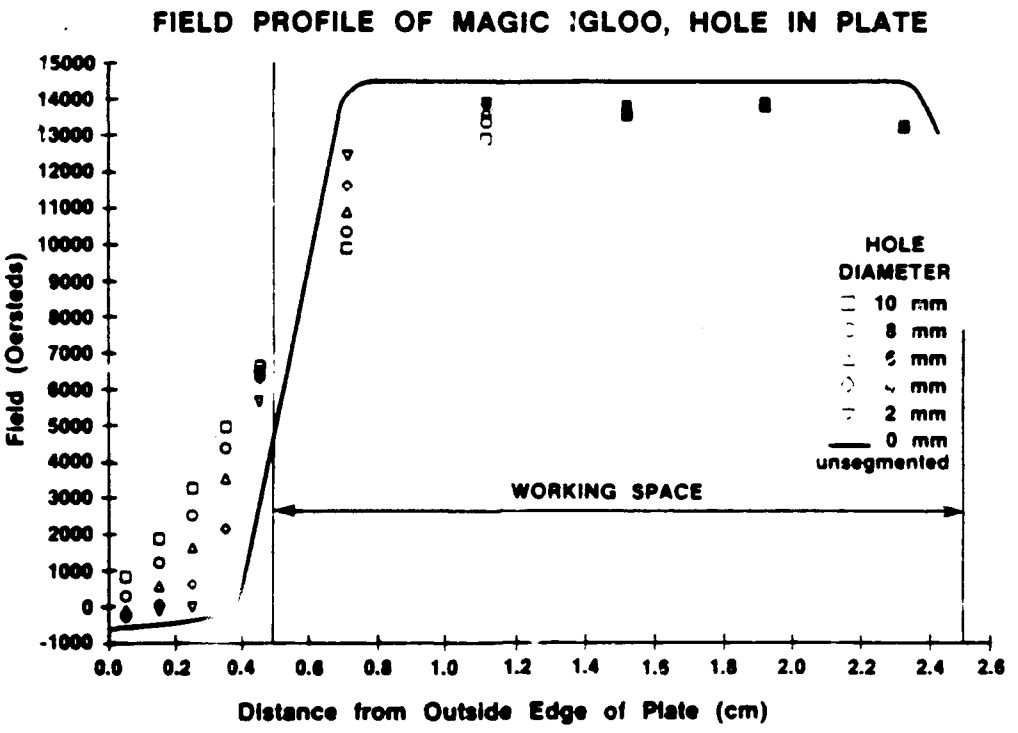

Figure 32. (A) Section of a hemisphere of a spherical field source like that of Fig. 30 rests on an iron slab which takes the place of the missing hemisphere. (B) On-axis field profile for access holes of different size.

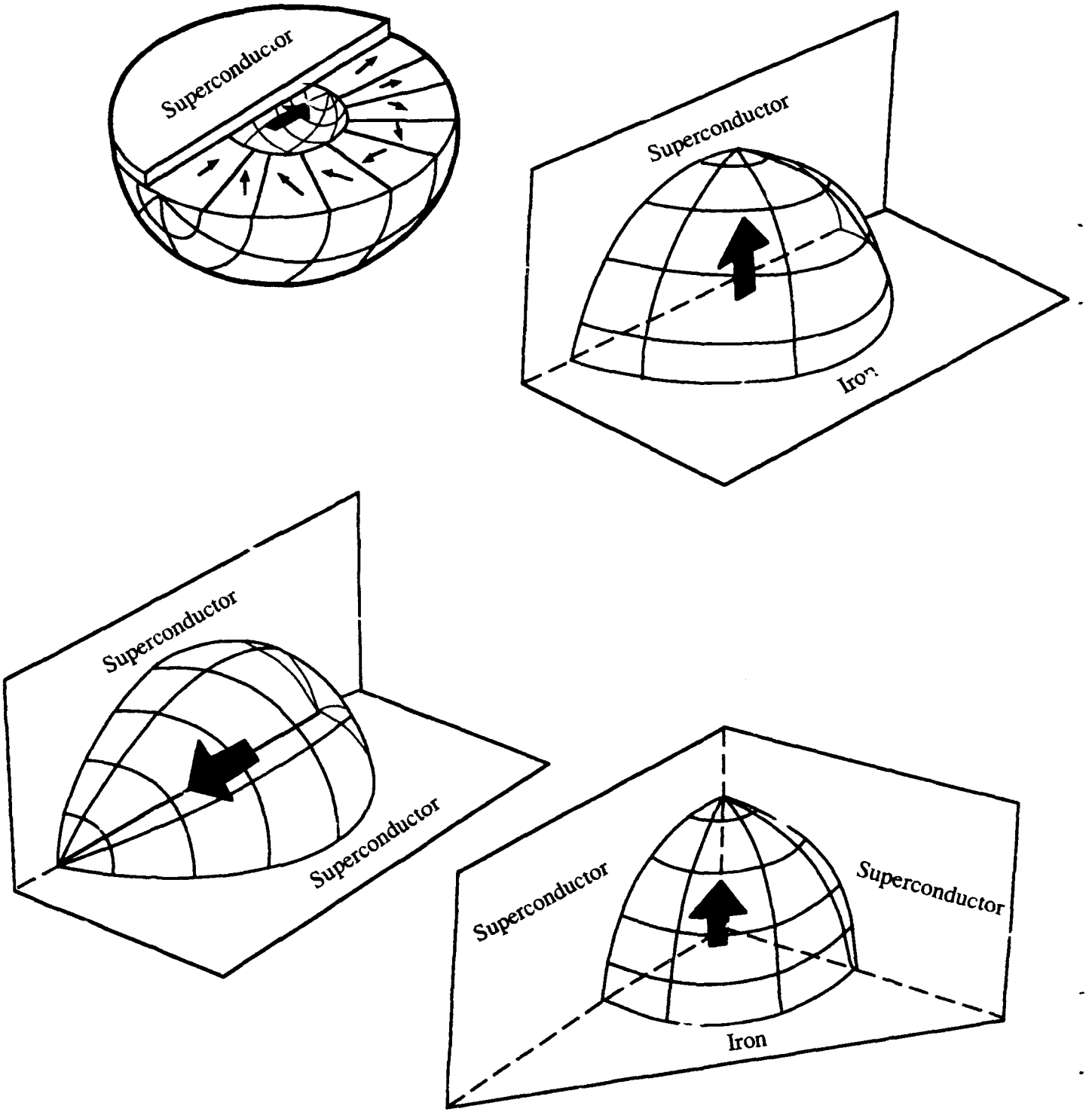

Figure 33. Hemi-, quarter-, and eighth-sphere structures that produce the same field as a complete sphere with magnetic mirrors (superconductors), and anti-mirrors (iron). For simplicity, only the exteriors and direction of polarity are shown in the last three figures.

Periodic Permanent Magnet Stacks (PPM's)

Field Sources for Travelling Wave Tubes

Travelling wave tubes are sources of microwave/millimeter wave radiation that employ an electron beam which is focussed and guided by an axial magnetic field. Sometimes the field is furnished by an electric solenoid but solenoids tend to be bulky and dependent on equally cumbersome power supplies. In military devices, especially airborne and ballistic ones, mass and bulk must be minimized. To obtain the necessary high field intensities in small-bore cylindrical structures, the fields are usually made periodic and are supplied by appropriate permanent magnet "stacks."[24-26] The simplest configuration is of the form shown in Fig. 34a where axially oriented magnets supply magnetic flux to the interior by way of interspersed iron pole pieces. Unfortunately, most of the the flux leaks to the exterior rather than passing through the bore where it is wanted. This difficulty can be ameliorated by indentation of the pole pieces at their external boundaries as in Fig. 34b. This is what is usually done,[27] and it is appropriate to refer to the configuration of Fig. 34b as the "conventional" stack. The rigid permanent magnets make alternatives to this arrangement possible. An obvious stratagem is to use only permanent magnets that are magnetized radially and are stacked to alternate between inward and outward orientations as in Fig. 35a. Such a stack is compared with the conventional array with regard to field and configurational bulk in Fig. 36. The comparison shows a significant advantage in favor of the radial magnet stack, especially in the technologically interesting region between 0.25 to 0.50 Teslas where a conventional stack must be as much as three times as massive to attain equal field with the same bore and period. A structure potentially still better is suggested by the transverse circular cylindrical magnets already discussed. There large fields are obtained through gradual linear variation of the magnetization orientation with the coordinate angle ϕ. If the change in orientation of the magnetization with distance x along the axis of the radial magnet stack is made to be gradual rather than in abrupt 180° jumps, the much improved field-bulk curve of Fig. 36 results. As in the case of the cylindrical magnets, the more practical 90° increments may be used with only about a 5% loss in field. See Fig. 35b. Here the bulk advantage over the conventional stack at the fields of interest is of an order of magnitude and more, especially at the higher fields where it is over two orders of magnitude. However, gradual variation of magnetization is not technologically feasible. Fortunately, as in the case of the rings, rather coarse orientation increments of 90° between adjacent segments produce a field ninety-four percent of that produced by the continuous variation. It is this insensitivity that changes the concept of gradual variation of orientation from an interesting speculative concept to a powerful technological tool.

Figure 37 shows the importance of high remanences in a "hybrid" configuration

which is composed of alternately stacked radially and axially oriented magnets. Included are curves showing the importance of remanence in the conventional stacks.

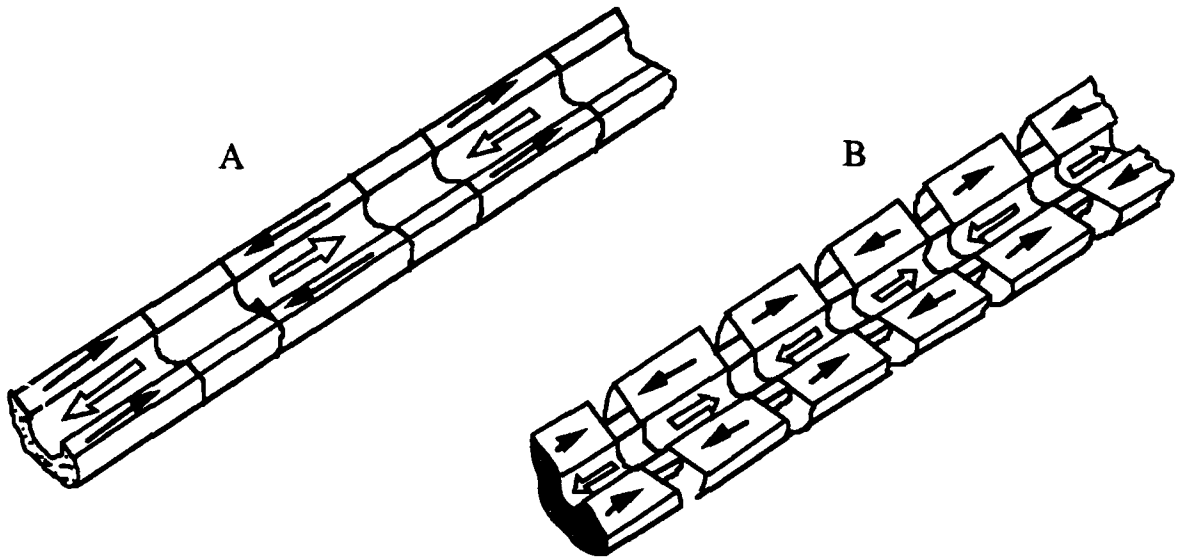

Figure 34. **A**. Simple PPM stack. **B**. PPM stack with indented pole pieces to reduce flux leakage to exterior.

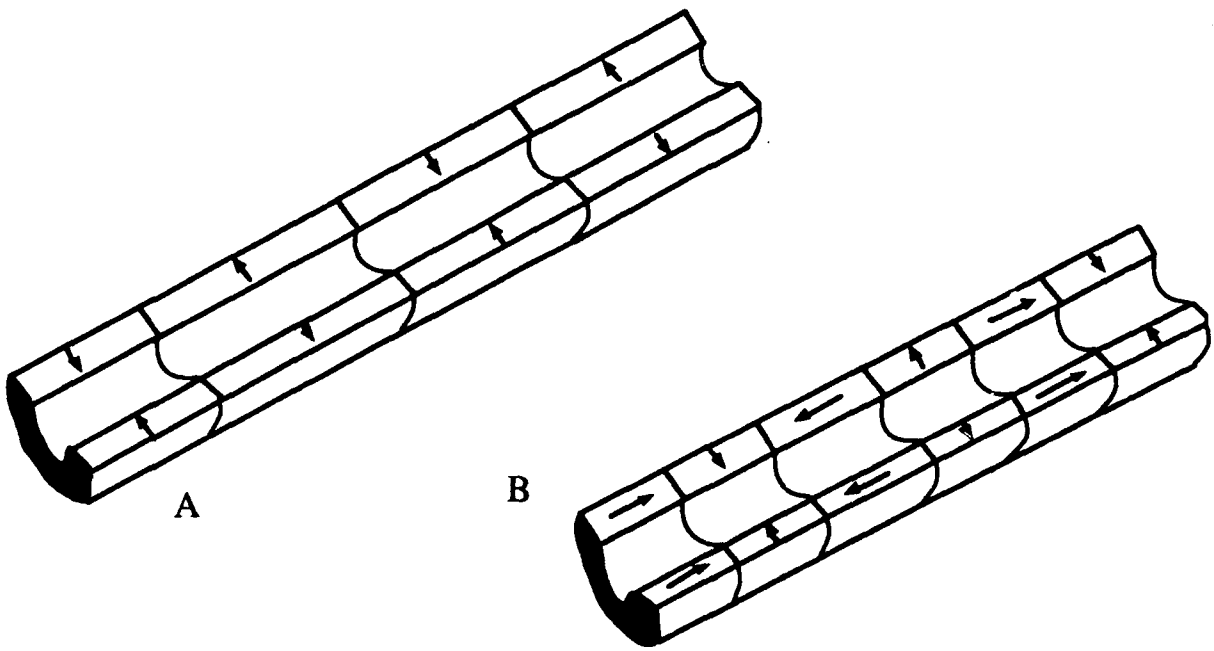

Figure 35. **A**. Radial PPM stack. **B**. Hybrid PPM stack.

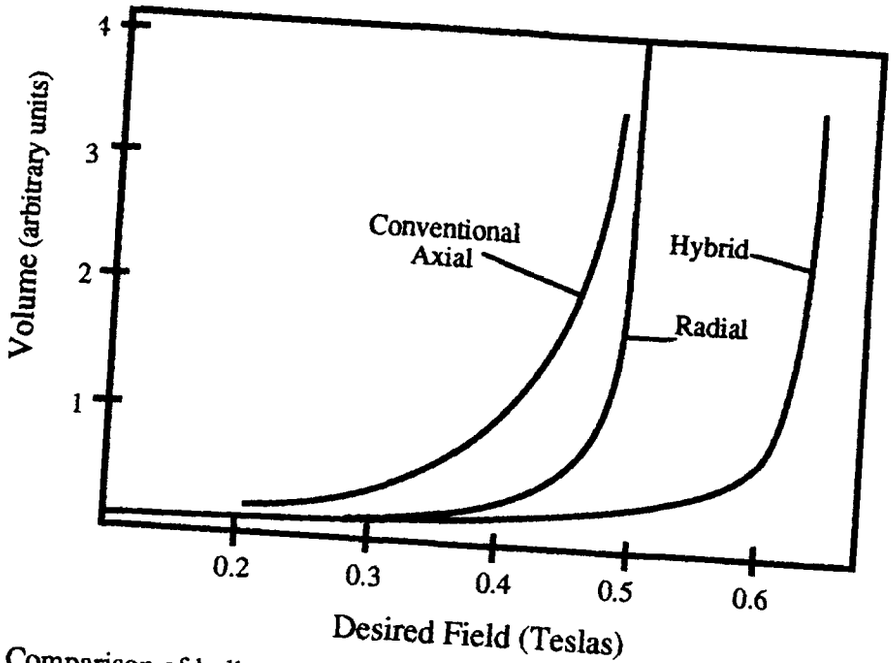

Figure 36. Comparison of bulks of structures of Fig. 35 with the conventional structure of Fig. 34b.

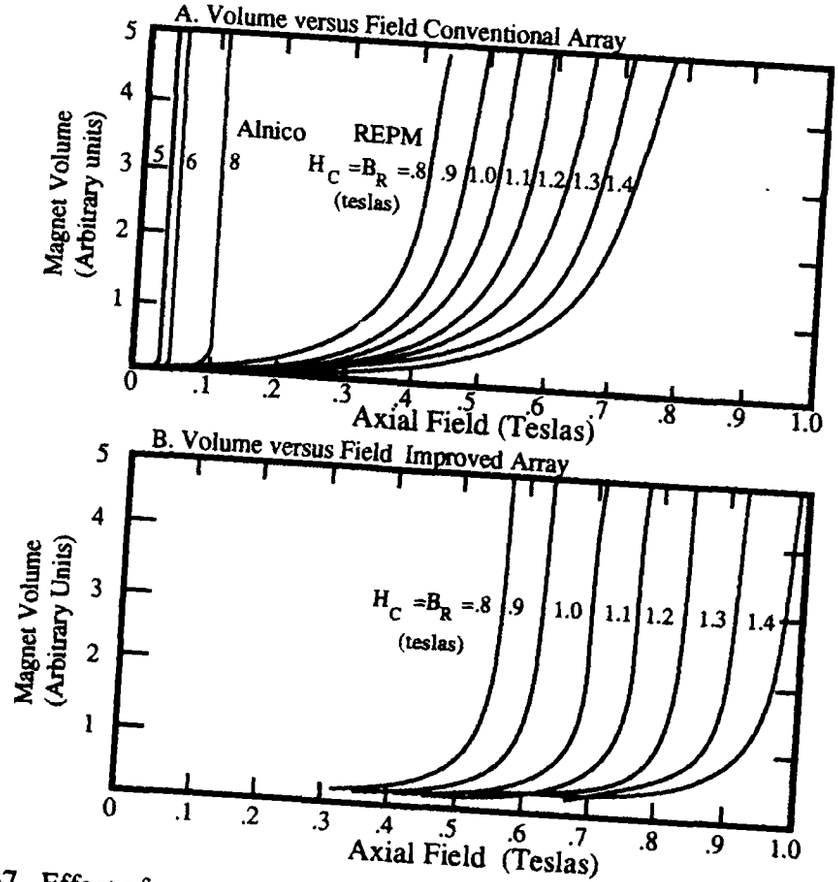

Figure 37. Effect of magnet remanence on structural bulk for two different arrays.

Curves for alnico are included to illustrate the futility of employment of the older magnet materials in designs where demagnetization coefficients are high.

Although the hybrid TWT magnets have impressive mass and field advantages over the conventional designs, they are at present more difficult to build for two reasons. First, it is hard to manufacture small-bore radially oriented ring magnets because of the difficulty of guiding sufficient flux through their bores to radially align and magnetize the high coercivity materials during manufacture. Secondly, because there are no iron pole pieces through which small amounts of perturbing flux can be conveniently forced to compensate for small field irregularities incurred in manufacture and assembly, all-magnet stacks are much harder to balance at present.

A simple and very effective alternative is to make pole pieces of triangular toroidal cross section as in Fig. 38.[28] This increases the magnetic permeance of the bore relative to that of the exterior so that more flux flows through the former. It also increases the average effective length of the axially oriented magnets, thereby increasing the magnetomotive force that drives the magnetic circuits. Both effects increase the field amplitude in the bore.

While it does not afford the spectacular mass and bulk advantages of the hybrid stack, the triangular poled array still possesses a significant bulk advantage of one to two over that of a conventional stack with indented poles at a bore field amplitude of 0.5 Tesla. Moreover, it has this advantage without incurrence of the manufacturing and balancing difficulties associated with the hybrid stack. It is probably the best all-around practical alternative at present.

As discussed in the previous section, extraordinarily high magnetic fields ($\approx$1.5 Teslas) are obtainable by placing spherical field sources in tandem. However, sources of such complexity are neither technologically nor financially viable given the present state-of-the-art.

Field Sources for Wigglers

Periodic transverse field sources are called wigglers and are used to provide lateral oscillatory motion to electron beams in free-electron lasers. It is this lateral acceleration that causes the electron to radiate. If the product of the flux density in Teslas and the wiggler period in centimeters is of the order of one or less, the beam will radiate coherently and laser action results. When this occurs, the wiggler is called an undulator.[29]

Some times the magnetic field is furnished by electromagnets with iron cores, but for the usual reasons these are generally not so desirable as permanent magnets. The simplest permanent magnet wiggler is just a series of bar magnets arranged as in Fig. 39a. More efficient would be planar arrays of magnets of alternately longitudinal and transverse orientation (see Fig. 39b). The principle used here is that of the hybrid TWT structure and as in that structure, a high field-to-mass ratio results. But like the TWT hybrid, it is somewhat difficult to adjust because of its lack of iron pole pieces to which

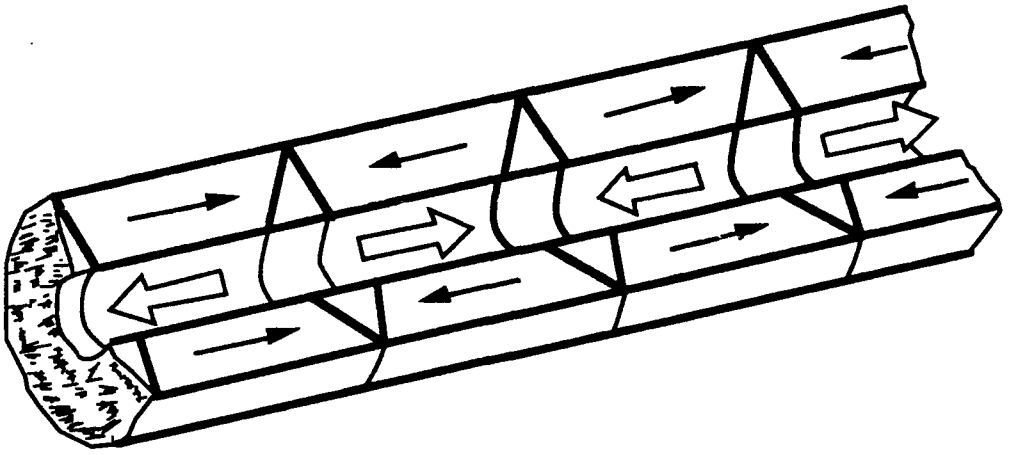

Figure 38. Section of conventional PPM stack with triangular section pole pieces. Large arrows indicate field directions in bore. Small arrows show directions of permanent magnet orientation.

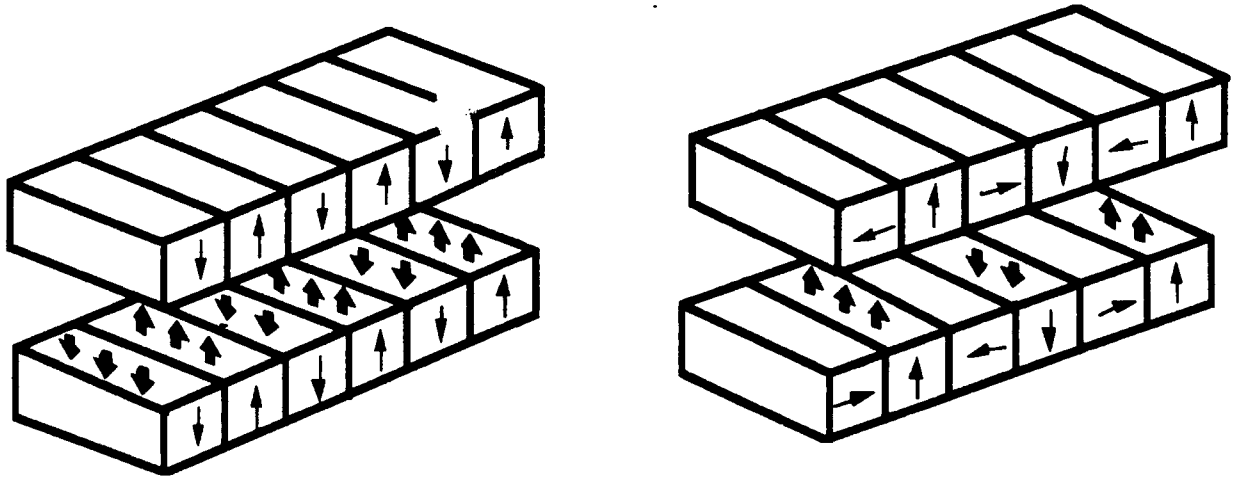

(a)

(b)

Figure 39. Simple wiggler structure, **a.** High field structure with 180° change in orientation of successive magnets, **b.** Hybrid structure with 90° change in orientation of successive magnets.

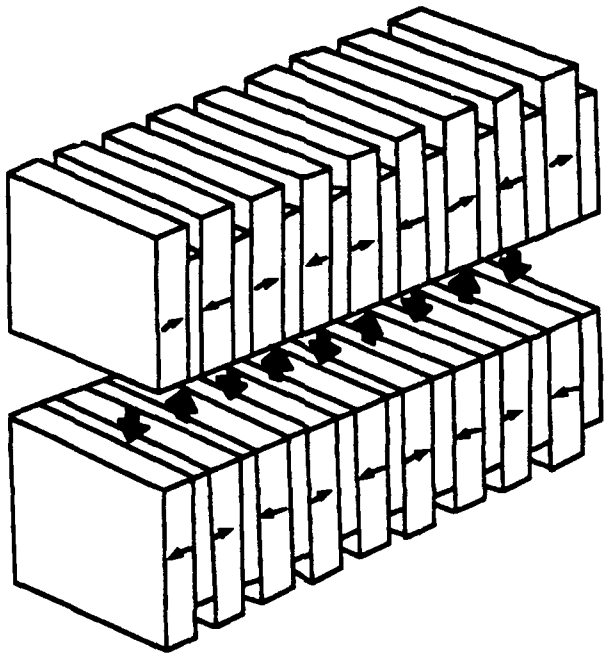

Figure 40. Stack with alternately oriented longitudinal magnet interspersed with indented iron pole pieces.

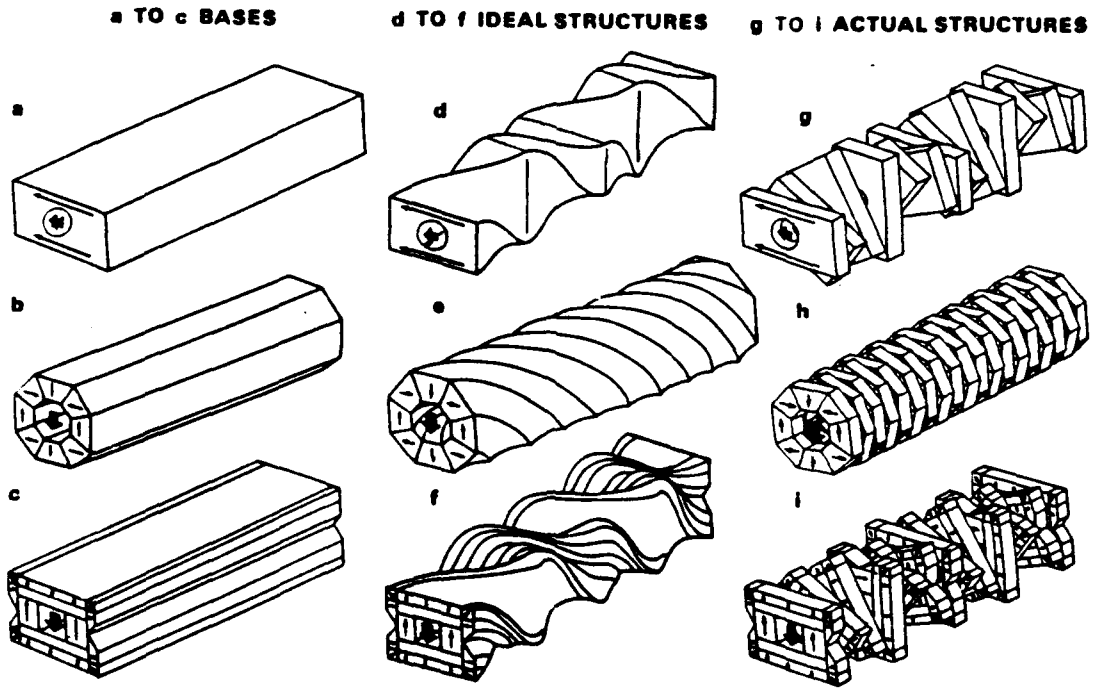

Figure 41. The three twister structures (**d-f**) with their respective transverse cylindrical bases (**a-c**) and their practical embodiments (**g-i**).

one can attach compensating shims. For this reason, the less bulk-efficient but more tractable arrangement of Fig. 40b is often used.[14] It can produce very high fields, is simple, relatively easy to adjust and probably the most practical choice where minimum mass and bulk is not a consideration.

Axial arrays of cross-sectional slices of any of the cylindrical transverse structures already discussed have the advantages of high-field capability and minimal flux leakage to the structural exterior, but they also suffer from relative complexity and inamenability to adjustments by shims. A possible partial solution would be use of slices of the mechanically adjustable rings. This would afford great flexibility in choice of field profile. Field strength, periodicity, and harmonic content could all be adjusted at will, but adjustment of local flaws would still be difficult compared with that of iron-yoked structures. Square frames could be compensated for local structural flaws but such compensation is also tedious compared to the rough and ready shimming and shunting of iron pole pieces.

Finally, spherical structures can be arranged transversely to produce a square-wave field pattern [26] with essentially zero-field gaps in the tunnels which are brought about by the large demagnetization coefficients of the cylindrical walls. As in the case of TWT's, average field strengths in such arrays are very high ($\approx$1.5 Teslas compared to the 0.05 - 0.50 Teslas of the typical wiggler) but, again, the structure is too complex and difficult to manufacture and compensate to be practical at present.

Twister Structures

The radiation from wigglers and undulators is polarized in the plane of the oscillatory motion of the electron beam. Sometimes it is desirable that the radiation be circularly polarized in which case a different magnetic array is needed to impart the necessary helical motion to the electron beam. This can be accomplished by employment of either a bifilar helical electric solenoid or by stacking a series of wiggler elements so that successive elements differ in orientation by a small angle ϕ. This results in a field that is constant in magnitude but whose orientation changes continuously with progression along the beam axis. Figure 41 shows such arrays together with the untwisted cylinders from which they are derived and the stacks of finite segments with which they are approximated in practice. The structures shown in Figs. 41b and 41c will be recognized as ones having already been discussed in cylindrical form. The structure in Fig. 41a is a simple, transversely magnetized bar magnet with a hole bored along its axes to accommodate the electron beam. The magnetic field in the hole is generated by the dipolar distribution on the inner surface that arises from the constant magnetization of the material. This field is slightly reduced by the presence of the more remote poles that the magnetization forms on the rectangular ends. The field is also progressively reduced with rate of twist and coarseness of twist increments. Fortunately, the effect of the latter is

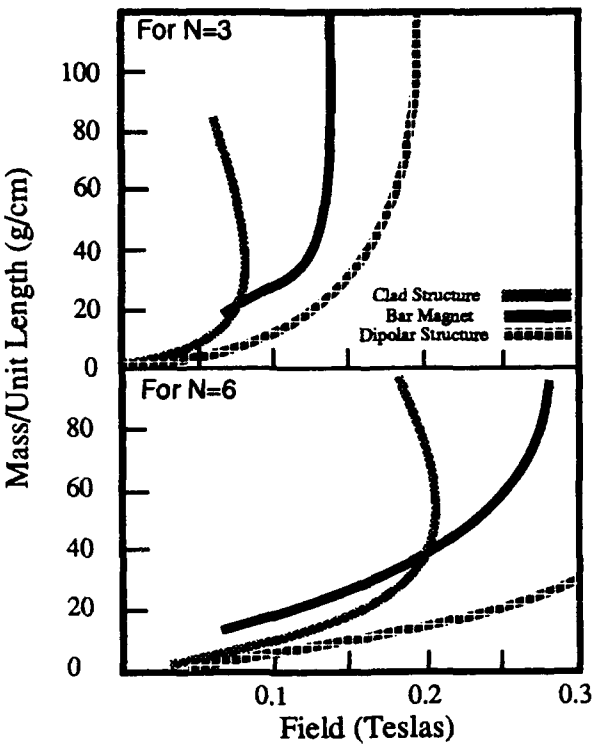

Figure 42. Structural mass as a function of field for two different period-to-bore ratios.

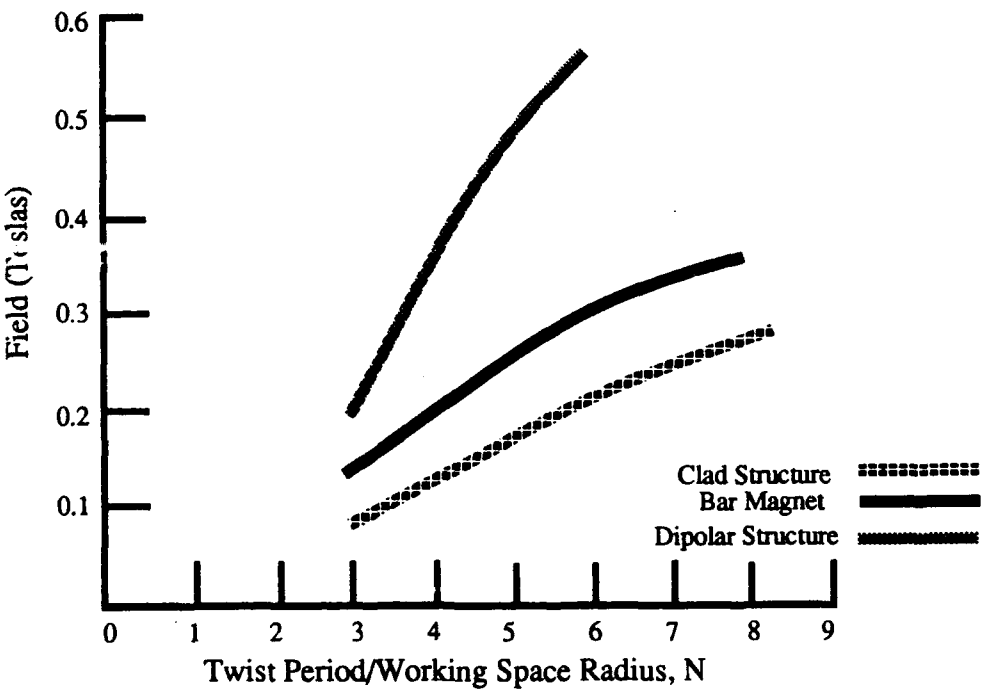

Figure 43. Maximum field attainable in three twister structures as a function of twist period to working space ratio.

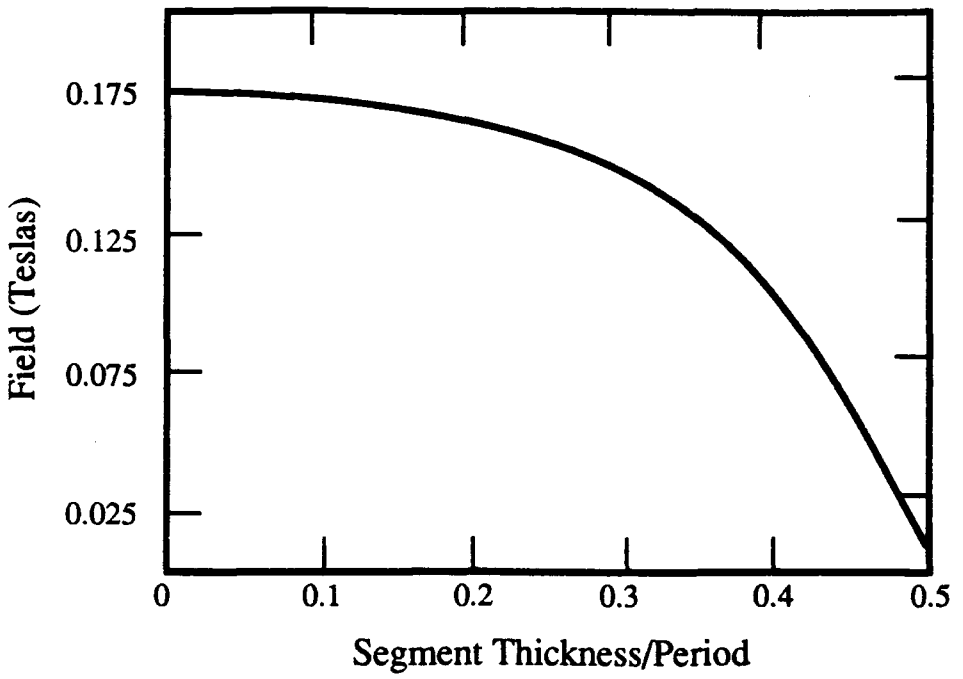

Figure 44. Maximum field attainable as a function of segment thickness/period ratio for the octagonal structure of Fig. 41b.

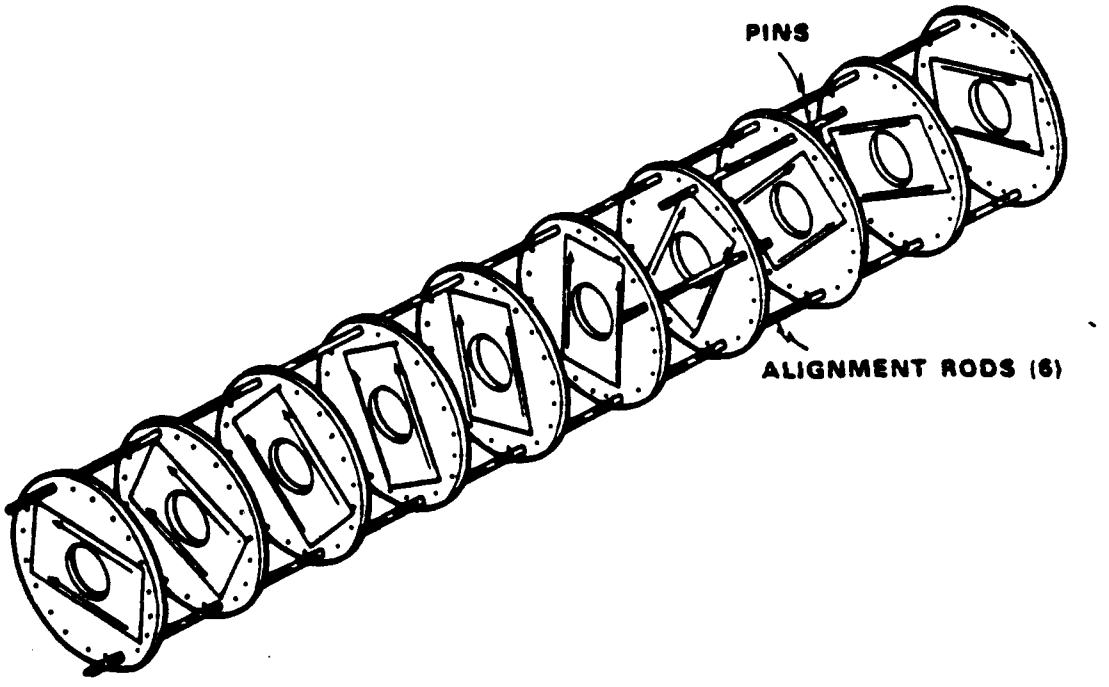

Figure 45. Exploded view of a twister prototype.

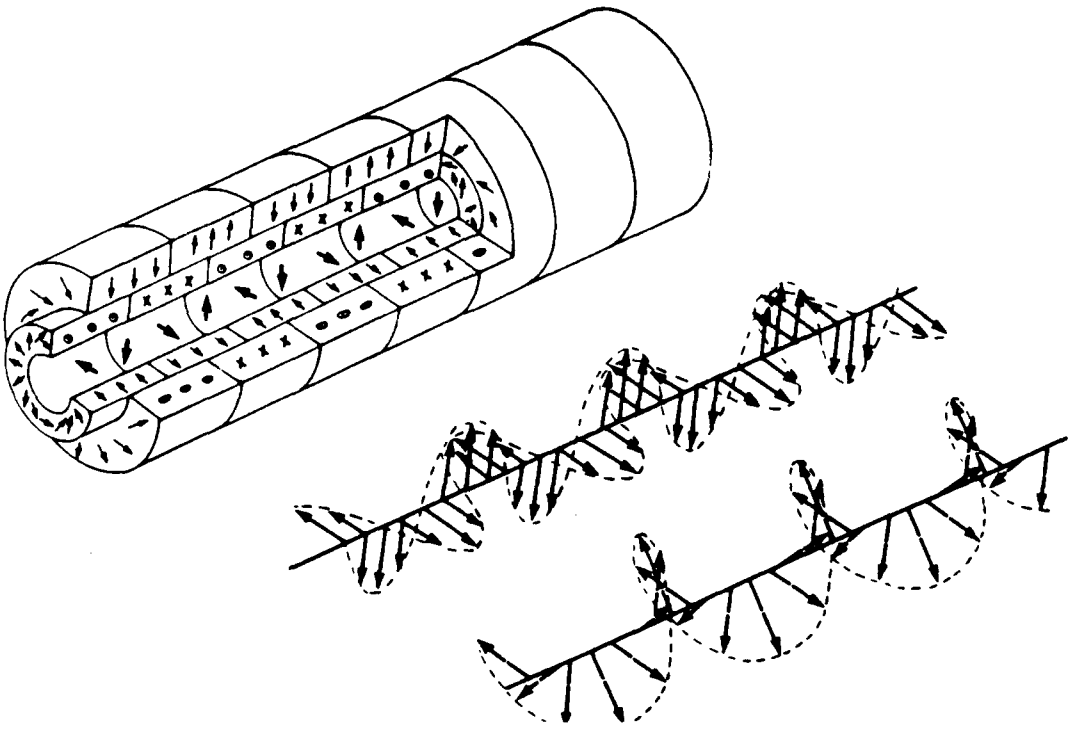

Figure 46. Addition of fields of two nested twisters to form a wiggler field.

small for reasonable increments. For example, the thirty-six degree change between successive segments used in a prototype results in a field diminution of the order of only one percent. Figures 42 through 44 compare the properties of the three structures with regard to parameters of interest. Although not quite so desirable as the structure of Fig. 41b, the simple bar magnet of Fig. 41a was chosen for a prototype design which is still far superior to the solenoid it will replace and less expensive than the other structures. The only advantage of the configuration in Fig. 41c is that the iron equipotential it forms tends to smooth aberrations in the material and structure to give a more uniform field. Otherwise the graphs of Figs. 42-44 show it to be less desirable than the other two and it is also by far the most expensive and difficult to manufacture.

The prototype was built and found to deliver the theoretical field of 0.13 Teslas compared to the 0.06 Teslas delivered by the presently employed solenoid with current of 200 amperes. Structural details are shown in Fig. 45. The magnet slices are mounted in brass discs for mechanical protection as the Sm_2Co_{17} of which they are composed is quite brittle. Rods through holes near the periphery of the brass mounts offer the proper alignment and provide flexibility in twist rate so that pitch can be adjusted or even varied with progression along the axis. The field strength and distribution agrees with the design specifications to about one percent.

A wiggler made up of field adjustable nested rings discussed in the previous

section affords an intriguing possibility. If the inner stack of such a structure is rotated by 90° and displaced one quarter period along the axis, its field will add vectorially with that of the outer ring to form the helical pattern of a twister (see Fig. 46). Thus, the adjustable ring wiggler is not only quantitatively adjustable, but can be operated as a twister of the same frequency as well.

Conclusions

While much progress has been made in REPM technology over the past two decades, the demand for certain improvements seems to be perenial.[2] As projected devices become more complex, the technological demands become more stringent. In this connection, achievement of the following would be very useful, and in some cases, critical:

(1) Better performance of temperature-compensated magnets. This includes further reduction of the already low-temperature coefficients of energy product and their extension to broader temperature ranges. Also important is the increase in energy products at all temperatures. Increases of the order of 25% would be attained by the squaring of the hysteresis loops alone. These developments are absolutely essential for the attainment of higher fields in smaller structures operating at greater power densities in TWT's projected for use in future lightweight, airborne devices. Raising the coercivities and squaring of the loops of the currently best Sm_2Co_{17} temperature-compensated magnets might be a solution. Compensation of the Nd-Fe-B compounds might be an even better one.

(2) Full magnet alignment in novel magnet geometries by getting sufficient flux where it is needed during the fabrication and magnetization processes. This can be very difficult in the case of conical shell magnets aligned normal to the cone surfaces, which would be very useful for the cladding of pole pieces in horseshoe-type magnetic circuits. Also difficult, for the same reason, is the radial magnetization of toroids with small holes and broad annuli.

(3) Improvement of fabrication and assembly techniques through the development and use of better solders, glues, epoxies, molds, presses, dies, etc. Routinization of details for fabrication of very unforgiving materials for better industry-wide standardization.

(4) A better variety of square-looped materials with low energy products is needed for widespread implementation of parametric field shaping. Possible approaches would be the development of very high coercivity ferrites, mischmetals, magnetically "knocked down" $SmCo_5$, SmCo's alloyed with heavy rare earths and composites of REPM's with solders or epoxies. Heat-resistant forms of the dilutants may also become very useful in the near future.

(5) Not directly connected with REPM technology, but potentially very important

for the intensification and broadening of their technological exploitation, are the development of innovative methods of heat handling. Included are both schemes for leading heat away from the thermally sensitive regions of devices, as well as improved resistance of materials to increased temperatures arising from miniaturization and increased power levels. Both retention and constancy of magnetic properties at high temperature are important.

(6) Investigation of deposition of REPM materials in the form of films on surfaces of different geometries should continue to be pursued.[29] Energy products must be raised, hysteresis loops squared, and mechanical and thermal ruggedness assured. Especially promising is the possibility of deposition of films of in-surface and normal-to-surface orientations upon each other. Success in such a venture could lead to a whole generation of small electronic devices that are unattainable at present.

(7) A keener awareness in the magnetic and industrial communities that the REPM's are more than just very powerful Alnicos. They afford not only the possibility of doing conventional tasks better, but offer a cornucopia of design options that were impossible before their advent. Still-prevalent mindsets acquired in the course of design experience with conventional magnets must be discarded when REPM's are used if the technological riches they offer are to be fully and speedily realized.

References

1. F. Rothwarf, L.J Jasper and H. A. Leupold, Proceedings of the Third International Workshop on Rare Earth-Cobalt Permanent Magnets and Their Applications, University of California, San Diego, June 27-30 (1978), p. 255; Proceedings book by University of Dayton, School of Engineering, Dayton, Ohio, USA, 45469

2. A. Tauber, H. A. Leupold and F. Rothwarf, Proceedings of the Eighth International Workshop on Rare Earth-Cobalt Permanent Magnets and Their Applications, Dayton, Ohio USA, May 5-9 (1985), p. 103

3. H. A. Leupold, Proceedings of the Fifth International Workshop on Rare Earth-Cobalt Permanent Magnets and Their Applications, Roanoke, Virginia USA, June 7-10 (1981), p. 270

4. Parker and Studders, *"Permanent Magnets and Their Applications,"* John Wiley and Sons, Inc., New York, London (1962)

5. H. C. Roters, *"Electromagnetic Devices,"* John Wiley and Sons, Inc., New York, and Chapman and Hall Ltd., London

6. H. A. Leupold , F. Rothwarf, C. G. Campagnoulo, H. Lee and J. E. Fine, *" Magnetic Circuit Design Studies for an Inductive Sensor,"* U.S. Army Technical Report, TR-ECOM-4158, October (1973) Fort Monmouth, New Jersey USA, 07703

7. W. Neugebauer and E. M. Branch, *"Applications of Cobalt-Samarium Magnets to Microwave Tubes,"* Technical Report, Microwave Tube Operations, General Electric, 15 March (1972), Schenectady, New York USA

8. J. P. Clarke and H. A. Leupold, IEEE Trans. Magn. **MAG-22**, No. 5, p.1063(1986)

9. H. A. Leupold and E. Potenziani II, IEEE Trans. Magn. **MAG-22**,No. 5, p.1078(1986)

10. H. A. Leupold, E. Potenziani II and J. P. Clarke, *"Shaping of Cylindrically Symmetric Magnetic Fields with Permanent Magnets,"* U.S. Army Technical Report, DELET-TR-84-12, December (1984), Fort Monmouth, New Jersey USA, 07703

11. J. P. Clarke, E. Potenziani II and H. A. Leupold, J. Appl. Phys. **61** (8), p. 3468(1987)

12. K. Halbach, Proceedings of the Fifth Internatio..al Workshop on Rare Earth-Cobalt Permanent Magnets and Their Applications, Roanoke, Virginia USA, June 7-10 (1981), p. 73

13. K. Halbach, Proceedings of the Eighth International Workshop on Rare Earth-Cobalt Permanent Magnets and Their Applications, Dayton, Ohio USA, May 5-9 (1985), p. 103

14. K. Halbach, Nucl. Instr. and Meth. **169**, p. 1 (1980)

15. A. B. C. Morcos, H. A. Leupold and E. Potenziani II, IEEE trans. Magn. **MAG-22**, No. 5, p. 1066 (1986)

16. H. A. Leupold, E. Potenziani II and M. G. Abele, J. Appl. Phys **64**, No. 10, p. 5994 (1988)

17. M.G. Abele, Technical Report, New York University School of Medicine, TR-14, 1 November 1986; H. A. Leupold, M. G. Abele and E. Potenziani II, J. Appl. Phys **67**, No. 9, p. 4644 (1990)

18. M. G. Abele, R. Chandra, H. Rusinek, H. A. Leupold and E. Potenziani II, IEEE Trans. Magn. **MAG-25**, No. 5, p. 39 (1989)

19. M. G. Abele and H. Rusinek, J. Appl. Phys. **67**, No. 9, p. 4644 (1990)

20. M. G. Abele, Technical Report, New York University School of Medicine, TR-20, 1 March 1989

21. M. G. Abele, Technical Report, New York University School of Medicine, TR-15, 1 March 1989

22. M. G. Abele and H. A. Leupold, J. Appl. Phys. **64**, No. 10, p. 5988 (1988)

23. H. A. Leupold and E. Potenziani II, J. Appl. Phys. **63** 8IIB, p. 3487 (1988)

24. H. A. Leupold, E. Potenziani II and A. Tauber, J. Appl. Phys. **67**, No. 9, p. 4656 (1990)

25. J. P. Clarke and H. A. Leupold, J. Appl. Phys. **63**, No. 8IIB, p.3991 (1988)

26. H. A. Leupold, W. D. Wilber and E. Potenziani II, IEEE Trans. Magn. **MAG-25**, No. 5, p. 3902 (1989)

27. J. E. Sterrett and H. Heffner, I. R. E. Trans. on Electron Devices **45**, p. 35 (1957)

28. M. G. Abele, Proceedings of the Tenth International Workshop on Rare-earth Magnets and Their Applications, Kyoto, Japan, 16-19 May(1990) p. 121; Proceedings Book by: The Society of Non-Traditional Technology, 1-2-8, Toranomon, Minato-Ku, Tokyo, 105 Japan

29. F. J. Cadieu, T. D. Cheung, L. Wickromasehara and S. H. Aly, J. Appl. Phys. **55**, No. 6, p. 2611 (1984)

ELECTRONICS TECHNOLOGY AND DEVICES LABORATORY
MANDATORY DISTRIBUTION LIST
CONTRACT OR IN-HOUSE TECHNICAL REPORTS

Defense Technical Information Center*
ATTN: DTIC-FDAC
Cameron Station (Bldg 5)
Alexandria, VA 22304-6145

(*Note: Two copies for DTIC will be sent from STINFO Office.)

Director
US Army Material Systems Analysis Actv
ATTN: DRXSY-MP
001 Aberdeen Proving Ground, MD 21005

Commander, AMC
ATTN: AMCDE-SC
5001 Eisenhower Ave.
001 Alexandria, VA 22333-0001

Commander, LABCOM
ATTN: AMSLC-CG, CD, CS (In turn)
2800 Powder Mill Road
001 Adelphi, Md 20783-1145

Commander, LABCOM
ATTN: AMSLC-CT
2800 Powder Mill Road
001 Adelphi, MD 20783-1145

Commander,
US Army Laboratory Command
Fort Monmouth, NJ 07703-5000
1 - SLCET-DD
2 - SLCET-DT (M. Howard)
1 - SLCET-DB
35 - Originating Office

Commander, CECOM
R&D Technical Library
Fort Monmouth, NJ 07703-5000
1 - ASQNC-ELC-IS-L-R (Tech Library)
3 - ASQNC-ELC-IS-L-R (STINFO)

Advisory Group on Electron Devices
201 Varick Street, 9th Floor
002 New York, NY 10014-4877

Director
Naval Research Laboratory
ATTN: CODE 2627
001 Washington, DC 20375-5000

Cdr, PM JTFUSION
ATTN: JTF
1500 Planning Research Drive
001 McLean, VA 22102

Rome Air Development Center
ATTN: Documents Library (TILD)
001 Griffiss AFB, NY 13441

Deputy for Science & Technology
Office, Asst Sec Army (R&D)
001 Washington, DC 20310

HQDA (DAMA-ARZ-D/Dr. F.D. Verderame)
001 Washington, DC 20310

Dir, Electronic Warfare/Reconnaissance
Surveillance and Target Acquisition Ctr
ATTN: AMSEL-EW-D
001 Fort Monmouth, NJ 07703-5000

Dir, Reconnaissance Surveillance and
Target Acquisition Systems Directorate
ATTN: AMSEL-EW-DR
001 Fort Monmouth, NJ 07703-5000

Cdr, Marine Corps Liaison Office
ATTN: AMSEL-LN-MC
001 Fort Monmouth, NJ 07703-5000

Dir, US Army Signals Warfare Ctr
ATTN: AMSEL-SW-OS
Vint Hill Farms Station
001 Warrenton, VA 22186-5100

Dir, Night Vision & Electro-Optics Ctr
CECOM
ATTN: AMSEL-NV-D
001 Fort Belvoir, VA 22060-5677

Cdr, Atmospheric Sciences Lab
LABCOM
ATTN: SLCAS-SY-S
001 White Sands Missile Range, NM 88002

Cdr, Harry Diamond Laboratories
ATTN: SLCHD-CO, TD (In turn)
2800 Powder Mill Road
001 Adelphi, MD 20783-1145